Time Reversal for MIMO Applications in Multipath Channels

A Project Report

submitted by

VAIBHAV

in partial fulfilment of the requirements
for the award of the degree of

Dual Degree (B.Tech + M.Tech)

DEPARTMENT OF Electrical Engineering
INDIAN INSTITUTE OF TECHNOLOGY MADRAS.

May 2018

THESIS CERTIFICATE

This is to certify that the thesis titled **Time Reversal for MIMO Applications in Multipath Channels**, submitted by **Vaibhav**, to the Indian Institute of Technology, Madras, for the award of the degree of **Dual Degree(B.Tech + M.Tech)**, is a bona fide record of the research work done by him under our supervision. The contents of this thesis, in full or in parts, have not been submitted to any other Institute or University for the award of any degree or diploma.

Dr. Ravinder David Koilpillai
Research Guide,
Professor,
Dept. of Electrical Engineering,
IIT-Madras, 600 036

Place: Chennai

Date: 30th May 2018

ACKNOWLEDGEMENTS

I would like to thank my guide, Professor R David Koilpillai for his constant guidance and support during the course of this project. His invaluable insights and suggestions made it possible for me to overcome every challenge faced during my work on this project. I am grateful to him for being patient with me while explaining the various nuances of communication systems that I was unaware of before working on this project. The two courses done under him played a major role in igniting my interest in Wireless Communications.

I would also like to thank the professors at Electrical Engineering Department for imparting the knowledge that has helped to transform me from a naive teenager with an interest in mathematics to a confident individual with an eye for engineering detail.

Finally, I would like to express my gratitude to my parents and my sister for standing by my side through the thick and thin of my life.

ABSTRACT

KEYWORDS: **Time Reversal, Alamouti, MIMO, OFDM , Cyclic Prefix, Decision Feedback based Interference Cancellation, ZF Equalizer**

In this thesis, a comprehensive study of Time Reversal processing for MIMO applications is presented. TR processing at the transmitter and at the receiver are separately studied and valuable insights are drawn from the simulations. For the case of TR processing at the transmitter, BER performance comparison between TR SIMO and TR MIMO is made which reveals TR MIMO performs better due to superior transmit diversity gain which is able to overpower the degradation due to increased Multi User Interference(MUI). ZF equalizer implemented at the receiver is able to improve the BER further, but upsampling at the transmitter before pulse shaping causes considerable overhead. To overcome this challenge posed by upsampling, we use OFDM w/o CP. In this case TR processing is done at the receiver. We begin by implementing OFDM w/o CP followed by TR and ZF equalizer using all $2L-1$ taps of the equivalent channel impulse response. Decision Feedback based Interference cancellation is implemented followed by ZF Equalizer based on L taps to replace the ZF equalizer based on $2L-1$ taps. This achieves a lower error floor compared to that achieved by ZF equalizer based on $2L-1$ taps presented in Farhang *et al.* (2016). For all the different implementations of TR MIMO, BER trend is studied by varying the channel length, equalizer taps and number of transmitters and receivers and the results are explained with the help of analytical expressions for Signal, Interference and Noise.

TABLE OF CONTENTS

LIST OF TABLES

LIST OF FIGURES

ABBREVIATIONS

TR	Time Reversal
MIMO	Multiple Input Multiple Output
SIMO	Single Input Multiple Output
ISI	Inter Symbol Interference
MSI	Multi Stream Interference
IBI	Inter Block Interference
MUI	Multi User Interference
BER	Bit Error rate
MLSE	Maximum Likelihood Sequence Estimation
CIR	Channel Impulse Response
UWB	Ultra Wide Band
AWGN	Additive White Gaussian Noise
CE	Channel estimation
ZF	Zero Forcing
DFIC	Decision Feedback based Interference Cancellation
MMSE	Minimum Mean Squared Error
SINR	Signal to Interference Noise Ratio
SNR	Signal to Noise Ratio
OFDM	Orthogonal Frequency Division Multiplexing
CP	Cyclic Prefix
DF	Decision Feedback
EM	Expectation-Maximization
dB	decibel
w/o	without

CHAPTER 1

INTRODUCTION

Time Reversal(TR), as the name suggests, is basically reversing the signal in time. In wireless communication systems, it stands for reversing the Channel Impulse Response(CIR) along with conjugation. The time-reversed CIR can either be used at the transmitter to precode the transmit signal or at the receiver for processing the received signal. The main advantage of TR processing is that it results in a high energy focussing effect (in time domain) at the receiver. The processing is similar to matched filtering in a dispersive channel. As a result, the signal can just be sampled at the receiver followed by low complexity equalizer or no equalizer at all. Although TR makes the equivalent channel response almost twice in length, its main energy term is present at the center of the equivalent (composite) response and the rest of the taps are of very low energy compared to the central tap. This phenomenon is called spatial-temporal focussing effect (see Aminjavaheri *et al.* (2017)). This is because TR technique harnesses the principle of channel reciprocity and multipath effects to concentrate the signal energy at a certain point in space (spatial focussing) and compress the CIR in the time domain (temporal focussing). It is well-known that radio signals experience multipath propagation due to the reflection from various scatters (interacting objects), especially in indoor environments. TR's focusing effect is in essence a spatial-temporal resonance effect that brings all the multipaths to arrive at a particular location at a specific moment. There has been considerable interest in exploiting this spatial-temporal focussing effect for MIMO communications in the recent years. We can get rich diversity benefit by employing large number of antennas at the base station in a MIMO system and there by get rid of or reduce the complexity the equalizer processing when TR is used. We now present the basic structure of TR-based communication to get a better understanding of the process.

1.1 Time Reversal Communication

TR Communication consists of two phases- Phase 1: Channel Probing and Phase 2: Data Transmission

Channel Probing Phase: In this phase the transceiver B sends out a pilot signal after pulse shaping with $p(t)$ to the transceiver A through the multipath channel with response $h(t)$. The received signal at transceiver A is basically the convolution of pulse shaped pilot signal and $h(t)$ (plus noise) which can be called $\tilde{h}(t)$. The received signal $\tilde{h}(t)$ can be treated as an equivalent channel response for the system.

Data Transmission Phase: Upon receiving the waveform, transceiver A time-reverses (and conjugate, when complex-valued) the received waveform $\tilde{h}(t)$, and uses the normalized TR waveform as a basic signature sequence $\tilde{g}(t)$

$$\tilde{g}(t) = \tilde{h}^*(-t) \tag{1.1}$$

The data to be transmitted is then convolved with this signature sequence to send it through the multipath channel.

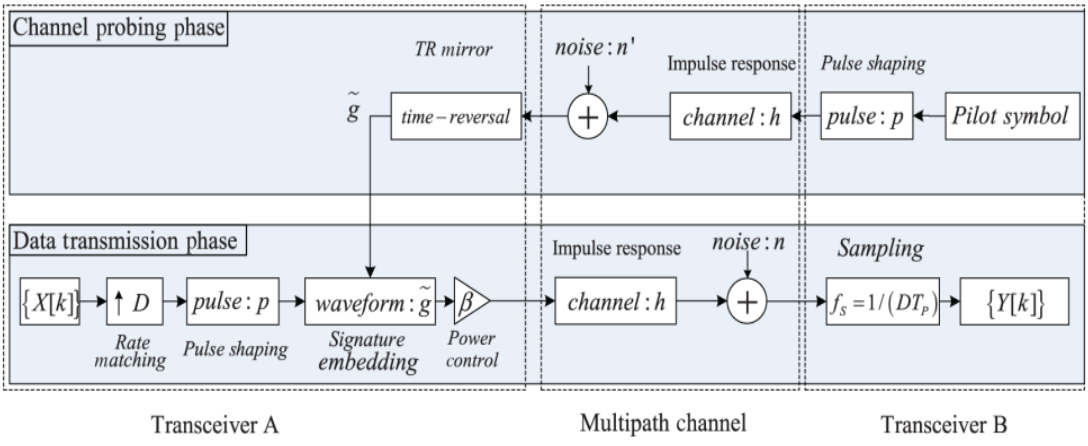

Figure 1.1: Basic Time Reversal Communication

There are two basic assumptions for the TR communication system to work.

1) Channel reciprocity: the impulse responses of the forward link channel and the reverse link channel are assumed to be identical.

2) Channel stationarity: the channel impulse responses (CIRs) are assumed to be stationary for at least one probing-and-transmission cycle.

We are interested in the Data Transmission phase of TR and do not study the Channel Probing phase in this thesis. Throughout this thesis, we assume perfect knowledge of the Channel State Information(CSI) at the base station where TR processing is carried out. Wherever necessary, we will make a comment about the channel estimation in the channel probing phase and suggest breifly the possible ways of tackling the challenges faced during channel estimation.

The TR technology was first introduced to compensate the delay distortion on wired transmission lines by Bogert (1957) from Bell Labs in the 1950s. It has been extensively studied and utilized in underwater acoustic channels with OFDM modulation by Edelmann *et al.* (2005) and Gomes and Barroso (2004). Another interesting application of TR technique is indoor localization or position detection Chen *et al.* (2016) where TR signatures of CIR from different locations in an indoor setting are correlated with the incoming signal to estimate the location from which the signal originated. Ray Liu and his team has been carrying out active research in this area. Some of the interesting solutions developed using time reversal by his team most recently include TR-Breath Chen *et al.* (2018) where TR technique is used to monitor the breathing rate of a person, TRIEDS Xu *et al.* (2017*b*) which deals with wireless event detection.

In this thesis, we present a comprehensive study of time reversal(TR) technique with an interest in BER performance of MIMO Communication system in multipath channels. The spatio-temporal focussing effect of TR can be revealed for large tap channels where the energy of the effective CIR is concentrated at the central tap, and remaining taps are of low energy as shown in Figure 1.2.

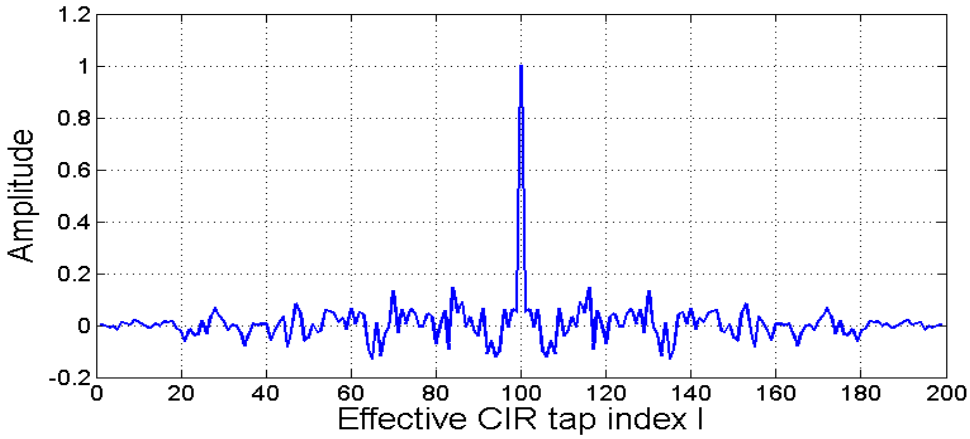

(a) $(h_1 \star g_1)[l]$

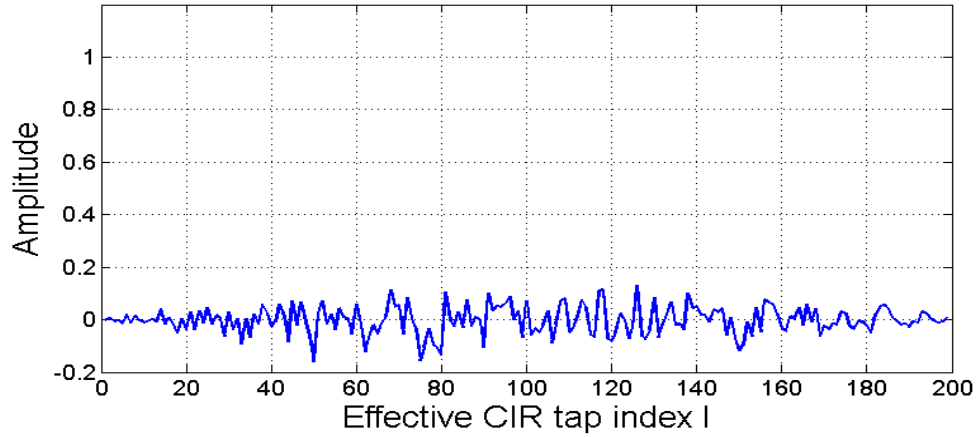

(b) $(h_1 \star g_2)[l]$

Figure 1.2: Correlation properties for 100 tap CIR

The remainder of this thesis is organized as follows: Chapter 2 describes initial study of Time Reversal application along with Alamouti Coding Scheme. Chapter 3 deals with TR MIMO system when the TR processing is done at the transmitter. Here we compare the TR SIMO and TR MIMO system performance in terms of BER and highlight the challenges faced when TR processing is done at the transmitter. Chapter 4 deals with TR MIMO system when TR processing is done at the receiver. Here we start with OFDM without CP and use TR processing to get rid of Inter Symbol Interference(ISI) and Multi Stream Interference(MSI). We also propose a decision feedback based interference cancellation technique to improve the performance of the system. The last Chapter describes the insights and conclusions drawn and suggests scope of future work. Simulation settings and results are present as the final section in each Chapter.

CHAPTER 2

Time Reversal in Alamouti Space Time Block Code

In the last Chapter, we introduced the concept of Time Reversal and mentioned a few applications for which it has been used in the field of wireless communications. The first step in this project was to study the behavior of TR in standard applications where it has been used. Keeping this in mind, a study of patent on "Time Reversal Space Time block Code" by Lindskog and Paulraj (2000) was carried out. This paper described how TR is used along with Alamouti coding scheme. This is a beginning step to understand the advantages of TR technique without having to deal with Multi Stream Interference. In this Chapter, we present implementation of a simple 2x1 system using Alamouti Scheme. At the receiver, a Viterbi MLSE Decoder in used to recover the sent bits. We conclude by presenting the simulation results for our 2x1 MISO system in Rayleigh fading channel, for cases with varying number of channel taps.

2.1 System Model

We begin by implementing 2x1 Alamouti scheme. Assume that the channel is a dispersive channel with multipath Rayleigh fading.

2.1.1 Channel Model

We assume an L-tap channel each with independent Rayleigh statistics. Let $\mathbf{h}_1[l] = [h_1[0], h_1[1], ..., h_1[L-1]$ be the equivalent discrete-time CIR between transmitter antenna 1 and receiver in discrete time and $\mathbf{h}_2[l] = [h_2[0], h_2[1], ..., h_2[L-1]$ be the CIR between transmitter antenna 2 and receiver. Here, channel tap $h_j[l]$ follows $\mathcal{CN}(0,1))$ for j = 1, 2 and $l \in [0, L-1]$.

2.1.2 System Description

In Alamouti coding scheme, we divide the transmit data into two blocks. Let $\mathbf{d}_1[l] = [d_1[0], d_1[1], ..., d_1[S-1]]$ be the first block and $\mathbf{d}_2[l] = [d_2[0], d_2[1], ..., d_2[S-1]]$ be the second block. We also divide the transmit period into two slots.

In time slot 1, $\mathbf{r}_1[l]$ is received at the receiver.

$$\mathbf{r}_1[l] = (\mathbf{h}_1 \star \mathbf{d}_1)[l] + (\mathbf{h}_2 \star \mathbf{d}_2)[l] + \mathbf{n}_1[l] \tag{2.1}$$

i.e., $\mathbf{d}_1[l]$ is trasmitted from transmit antenna 1 and $\mathbf{d}_2[l]$ is trasmitted from transmit antenna 2. $\mathbf{n}_1[l]$ is the AWGN signal at the receiver in time slot 1.

i.e., slot 2, $\mathbf{r}_2^{'}[l]$ is received at the receiver.

$$\mathbf{r}_2^{'}[l] = -(\mathbf{h}_1 \star \mathbf{d}_2^*)[l] + (\mathbf{h}_2 \star \mathbf{d}_1^*)[l] + \mathbf{n}_2[l] \tag{2.2}$$

That is $-\mathbf{d}_2^*[l]$ is transmitted from transmit antenna 1 and $\mathbf{d}_1^*[l]$ is transmitted from transmit antenna 2. $\mathbf{n}_2[l]$ is the AWGN signal at the receiver in time slot 2. The received signal samples $\mathbf{r}_2^{'}[l]$ are then complex conjugated giving the signal $\mathbf{r}_2[l]$

$$\mathbf{r}_2[l] = \left(\mathbf{r}_2^{'}[l]\right)^* = -(\mathbf{h}_1^* \star \mathbf{d}_2)[l] + (\mathbf{h}_2^* \star \mathbf{d}_1)[l] + \mathbf{n}_2^*[l] \tag{2.3}$$

Taking the Z-transform of the above equations (2.1) and (2.3) makes it easier to write them in matrix notation by transforming the convolution operation into a simple product term.

Let $\mathbf{r} = [\mathbf{r}_1(z)\ \ \mathbf{r}_2(z)]^T$, $\quad \mathbf{d} = [\mathbf{d}_1(z)\ \ \mathbf{d}_2(z)]^T$, $\quad \mathbf{n} = [\mathbf{n}_1(z)\ \ \mathbf{n}_2(z)]^T$ then

$$\mathbf{r} = \mathbf{H}\mathbf{d} + \mathbf{n}, \tag{2.4}$$

where

$$\mathbf{H} = \begin{bmatrix} \mathbf{h}_1(z) & \mathbf{h}_2(z) \\ \mathbf{h}_2^*(z) & -\mathbf{h}_1^*(z) \end{bmatrix} \tag{2.5}$$

We need to find a matrix that is orthogonal to $\mathbf{H}$. Let $\mathbf{H}^H$ be the matrix that is

orthogonal to $\mathbf{H}$.

$$\mathbf{H}^H\mathbf{H} = \big(|\mathbf{h}_1|^2 + |\mathbf{h}_2|^2\big)I, \tag{2.6}$$

$$\mathbf{H}^H = \begin{bmatrix} \mathbf{h}_1^*(z) & \mathbf{h}_2(z) \\ \mathbf{h}_2^*(z) & -\mathbf{h}_1(z) \end{bmatrix} \tag{2.7}$$

Note: Here we are not normalizing the time-reversed version of the CIR by the channel energy. This is contrary to the TR for MIMO systems implemented in Chapter 3 and Chapter 4, where the time-reversed version of the CIR, used for precoding the data and post processing the received signal respectively, is normalized by the corresponding channel energy.

Alamouti proposes to multiply $\mathbf{r}$ with $\mathbf{H}^H$ at the receiver to obtain the signal $\mathbf{x} = [\mathbf{x}_1 \quad \mathbf{x}_2]^T$

$$\begin{aligned} \mathbf{x} = \mathbf{H}^H\mathbf{r} &= \mathbf{H}^H\mathbf{H}\mathbf{d} + \mathbf{H}^H\mathbf{n} \\ &= \big(|\mathbf{h}_1|^2 + |\mathbf{h}_2|^2\big)\mathbf{d} + \hat{\mathbf{n}}, \end{aligned} \tag{2.8}$$

where $\hat{\mathbf{n}} = \mathbf{H}^H\mathbf{n} = [\hat{\mathbf{n}}_1 \;\; \hat{\mathbf{n}}_2]^T$.

$\mathbf{x}_1$ and $\mathbf{x}_2$ are given by

$$\mathbf{x}_1 = \big(|\mathbf{h}_1|^2 + |\mathbf{h}_2|^2\big)\mathbf{d}_1(z) + \hat{\mathbf{n}}_1 = \big(\mathbf{h}_1^*(z)\mathbf{h}_1(z) + \mathbf{h}_2^*(z)\mathbf{h}_2(z)\big)\mathbf{d}_1(z) + \hat{\mathbf{n}}_1 \tag{2.9}$$

$$\mathbf{x}_2 = \big(|\mathbf{h}_1|^2 + |\mathbf{h}_2|^2\big)\mathbf{d}_2(z^{-1}) + \hat{\mathbf{n}}_2 = \big(\mathbf{h}_1^*(z)\mathbf{h}_1(z^{-1} + \mathbf{h}_2^*(z)\mathbf{h}_2(z^{-1})\big)\mathbf{d}_2(z^{-1}) + \hat{\mathbf{n}}_2 \tag{2.10}$$

Let us take an example of 2-tap channel,

$$\mathbf{h}_1(z) = h_{10} + h_{11}z^{-1} \qquad \mathbf{h}_2(z) = h_{20} + h_{21}z^{-1} \tag{2.11}$$

$$\mathbf{h}_1^*(z) = h_{10}^* + h_{11}^*z \qquad \mathbf{h}_2^*(z) = h_{20}^* + h_{21}^*z \tag{2.12}$$

Therefore, the equivalent CIR given by $\left(|\mathbf{h}_1|^2 + |\mathbf{h}_2|^2\right)$ is

$$\left(|\mathbf{h}_1|^2+|\mathbf{h}_2|^2\right) = \Big((|h_{10}|^2+|h_{11}|^2+|h_{20}|^2+|h_{21}|^2)+(h_{10}h_{11}^*+h_{20}h_{21}^*)z+(h_{10}^*h_{11}+h_{20}^*h_{21})z^{-1}\Big) \tag{2.13}$$

From the above eqn.(2.13), we can see that there are 2 Inter Symbol Interference (ISI) terms in the expression which can limit the performance of the system apart from the noise terms. To counter the effect of these ISI terms, we implement a Viterbi MLSE Decoder described in Bottomley and Chennakeshu (1998) at the receiver after $\mathbf{x}_1$ and $\mathbf{x}_2$ have been generated. To summarize, for an L- tap channel, the effective channel response will be that of $(2L-1)$ tap channel with the central tap being the Real power term of interest to us. The remaining $(2L-2)$ taps ($L-1$ to the left and $L-1$ to the right of the central real term) contribute to the ISI.

2.1.3 Viterbi MLSE Detector

In order to recover the sent bits, implemented a MLSE Viterbi decoder was at the receiver. When using MLSE Decoder, the estimated symbol sequence $\hat{\mathbf{d}}_1[l]$ will be the sequence that maximizes the recursively defined matched filter metric

$$\begin{aligned} Metric(l) = Metric(l-1) + \Big|\mathbf{x}_1[l] - \big((h_{10}h_{11}^* + h_{20}h_{21}^*)\hat{\mathbf{d}}_1[l] \\ +(|h_{10}|^2 + |h_{11}|^2 + |h_{20}|^2 + |h_{21}|^2)\hat{\mathbf{d}}_1[l-1] \\ +(h_{10}^*h_{11} + h_{20}^*h_{21})\hat{\mathbf{d}}_1[l-2]\big)\Big| \end{aligned} \tag{2.14}$$

Note that the above metric is defined for the case of 2-tap channel.

For an L-tap channel, the effective channel after TR processing has $(2L-1)$ taps. And the number of states for $(2L-1)$ tap channel MLSE Viterbi decoder is $2^{(2L-2)}$ for BPSK modulation. Therefore, for every tap increase in channel response, the complexity of the decoder increase by a factor of 2^2. This incurs a lot of processing delay. The complexity is tabulated below in Table 2.1.

This posed a major challenge in terms of writing a generalized MLSE decoder code that would work for any channel length. Such a program was written- $Alamouti\_viterbi\_universal.m$ which takes in the number of channel taps, number

of total bits as inputs and produces the recovered bits and BER curve as output. The simulations results are discussed in the next section.

L	Effective Taps 2L-1	no. of ISI terms 2L-2	no. of states in MLSE 2^{2L-2}
1	1	0	1
2	3	2	4
3	5	4	16
4	7	6	64

Table 2.1: Complexity of MLSE Viterbi Decoder with number of channel taps L

2.2 Simulation Results

In this section, we present the simulation results for 2-tap and 3-tap channels. Simulations were carried out for a total of 10^6 bits, assuming that the channel response does not change for a block of 100 bits. These 100 bits block was then divided into two sequence sets $\mathbf{d}_1[l]$ and $\mathbf{d}_2[l]$ as needed for Alamouti code.

For a two-tap channel, the BER performance was not as expected. This led to an inquiry about the nature of errors in the recovered bit. I noticed that most of the errors occurred at the end of the block over which MLSE detector was being run. This is demonstrated in the error plot shown below.

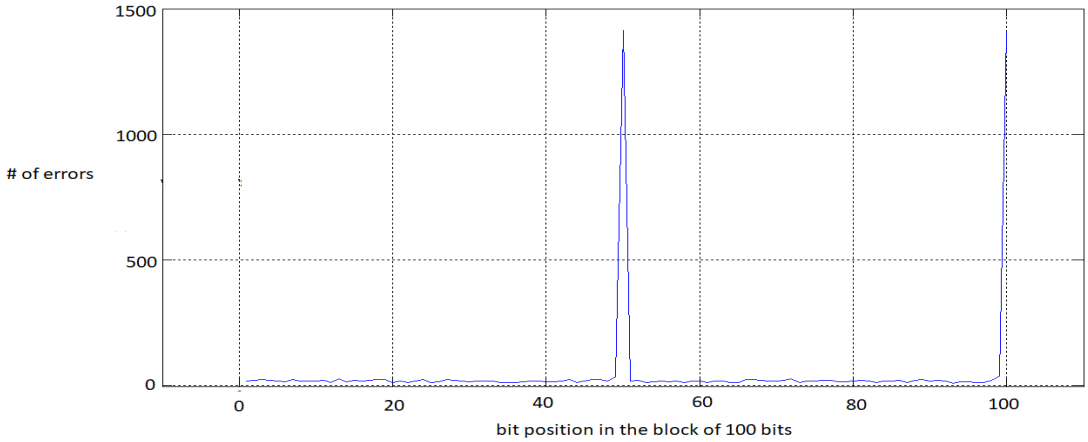

Figure 2.1: Error plot wrt. bit position in block of 100 bits

Notice that number of errors reaches peak value at around the 50^{th} and 100^{th} bits, which are the end of the blocks for which MLSE is run. As a result, (2L-2) zeros were padded at the beginning and end of each block as suggested by my advisor. Upon

detection, the recovered bits corresponding to the padded zeros are discarded and this improved the BER performance.

Figures 2.2(a) and 2.2(b) shows the BER performance of the 2 tap and 3 tap channels respectively. As expected, it follows the theoretic BER performance of 4-branch MRC and 6-branch MRC.

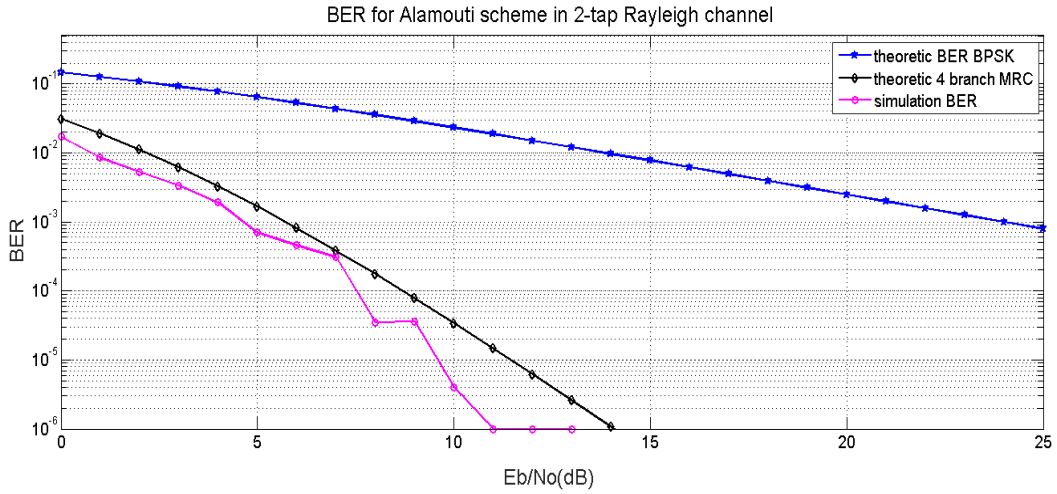

(a) 2 tap channel

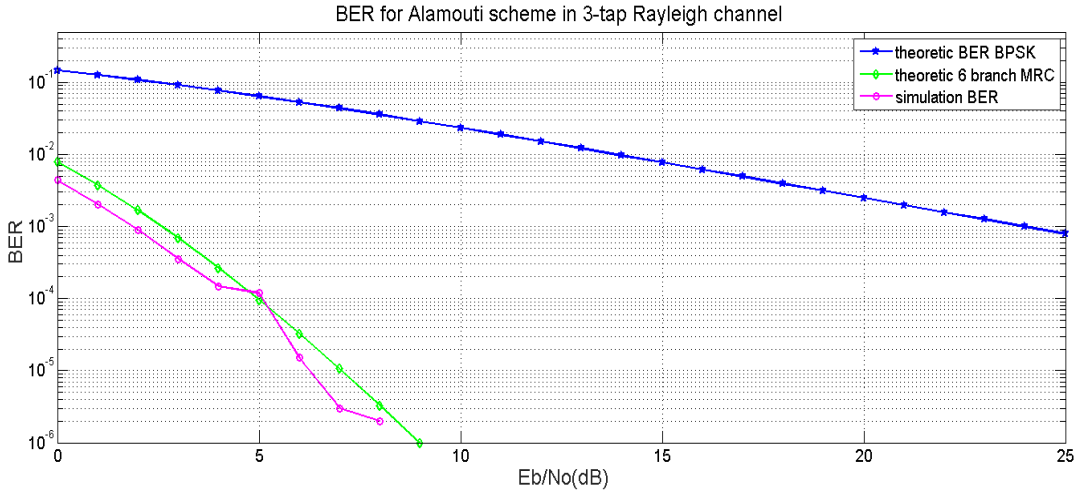

(b) 3 tap channel

Figure 2.2: Alamouti 2x1 scheme

In the Figure 2.2(b), the diversity benefit compared to that in figure 2.2(a) is due to 6 terms in $(|h_{10}|^2 + |h_{11}|^2 + |h_{12}|^2 + |h_{20}|^2 + |h_{21}|^2 + |h_{22}|^2)$. Here we have not normalized the time reversed channel response, hence we are able to see the diversity benefit compared to 2-tap channel. If we had normalized the time reversed channel response, then this term would have been equal to 2.

Although we can go ahead and simulate for larger number of channel taps L, but for large number of channel taps, the MLSE Viterbi decoders complexity increases exponentially as discussed in the previous section. As a result, the system takes a lot time to yield the simulation results.

From the above implementation of the 2x1 Alamouti scheme proposed by Lindskog and Paulraj (2000), we can see that the diversity benefit on increasing the channel length is a direct consequence of not normalizing the time reversed channel response. Whereas in the implementation of TR MIMO system in the next Chapter, we see that the time reversed channel response used to precode the data is normalized by the respective channel energy.

The possible justification for not normalizing the time reversed channel response is because of the absence of Multi Stream interference (MSI) terms. The beauty of Alamouti scheme is that the two data streams $\mathbf{d}_1[l]$ and $\mathbf{d}_1[l]$ are recovered without any interference from each other(although there still remains ISI). This makes sure that the MSI energy is not greater that the main tap energy as MSI is not present. Whereas in TR MIMO system we need to normalize the time reversed channel response used for precoding the data because there are MSI terms present in the system. If we do not normalize the time reversed channel response then the MSI channel coefficients can become larger than the main tap of the channel of interest. This defeats the purpose of TR where the central tap of the effective channel response is of very high energy and all the rest ISI and MSI taps are of very low value. More will be discussed about this issue in the next two chapters.

CHAPTER 3

TR processing at Transmitter

In the last Chapter,we saw how Time Reversal (TR) technique is used along with Alamouti space time coding scheme and analyzed the BER performance by increasing the number of channel taps for a simple 2x1 system. Since an MLSE Viterbi decoder is used at the receiver to recover the transmitted signal, it is not feasible for a channel which has a large delay spread (compared to the sampling period) and hence a large number of channel taps. In this Chapter we will look at the BER performance of SIMO system when data is precoded by the TR waveform at the transmitter. We then compare the results obtained with that of MIMO system where spatial multiplexing of data is employed to achieve transmit diversity. We use the same channel model as described in Chapter 1 of this thesis. A description of the system model is first presented for downlink communication and analytical expressions for the received signal are derived. We then carry out simulations to get BER performance of the TR system under various scenarios by changing the number of channel taps, number of receivers and number of transmitters. We compare these results with the case when ZF equalizer is used at the receiver. We also show that, although the noise is augmented by the spatial multiplexing in TR MIMO scheme, this is overshadowed by the substantial transmit diversity achieved.

3.1 TR SIMO Downlink Communication

In this section we consider a time-reversal downlink system where there is a single transmitter and M receiver antennas. Here the single transmitter antenna is present at the base station and M receivers can be thought of as mobile stations for our SIMO Downlink communication system. The implementation of this SIMO system is adapted from TRDMA system described in Han *et al.* (2016).

3.1.1 Channel Model

Suppose there are V_{max} independent multipaths from the transmitter to the m^{th} receiver, then the channel $h_m(t)$ can be written as

$$h_m(t) = \sum_{v=1}^{V_{max}} \tilde{h}_{m,v}\delta(t - \tau_v) \tag{3.1}$$

where $\tilde{h}_{m,v}$ and τ_v are the complex channel gain and path delay of the v^{th} path, respectively. Note that the delay spread of the channel is given by $\tau_C = \tau_{V_{max}} - \tau_1$.

Let W be the bandwidth of TR system. Through Nyquist sampling , the discrete channel response is

$$h_m[n] = \int_{n\tau_p - \tau_p}^{n\tau_p} p(n\tau_p - \tau)h_m(\tau)d\tau \tag{3.2}$$

where $p(t)$ is the pulse with main lobe $\tau_p = 1/W$.

Through eqn.(3.2), a L-tap channel

$$\mathbf{h}_m = [h_m[0], h_m[2], ..., h_m[L-1]]^T \tag{3.3}$$

with $L = round(\tau_C W)$ can be resolved for the link between the transmitter and the m^{th} receiver where $h_m[i]'s$ are independent for all $i \in [0, L-1]$ and $m \in [0, M-1]$.

As mentioned in the last Chapter, throughout this thesis we assume that the BS has a perfect knowledge of the CSI. For the purpose of simulations, the CIRs are modeled as FIR filters with length L. The multipath channel tap $h_j[l]$ follows $\mathcal{CN}(0, \rho(l))$ to imitate Rayleigh fading taps, where $\rho(l)$ depends on the power delay profile of the channel model.

3.1.2 System Model

In this SIMO system, the transmitter simultaneously communicates with all the M receivers. The data to be transmitted is first pulse shaped by pulse shaping filter. In our simulations, SRRC pulse is used as the pulse shaping filter with a bandwidth B=200 MHz. Ideally, the symbols should be present at symbol spaced points after pulse shap-

ing ie., at distance of $T_s = 1/B$ where B is the bandwidth of the pulse shaping filter, but in order to suppress the Inter Symbol Interference (ISI) caused by the multipath channel, the symbols are first upsampled by a factor D, and then sent through the pulse shaping fitler. Here D is chosen such that the main lobes of the pulse corresponding to two consecutive symbols is atleast 3 symbol durations apart. This is one of the major drawbacks of the TR SIMO and TR MIMO communication system described in Han *et al.* (2016) and Nguyen *et al.* (2009) respectively. X_m denotes the data to be transmitted to the m^{th} receiver for all $m \in [0, M-1]$ after pulse shaping. After pulse shaping, all the signals to different receivers are mixed as follows.

$$S[k] = \sum_{m=0}^{M-1} (X_m \star g_m)[k], \tag{3.4}$$

where

$$g_m[l] = \frac{h_m^*[L-1-l]}{\sum_{i=0}^{L-1} |h_m[i]|^2} \tag{3.5}$$

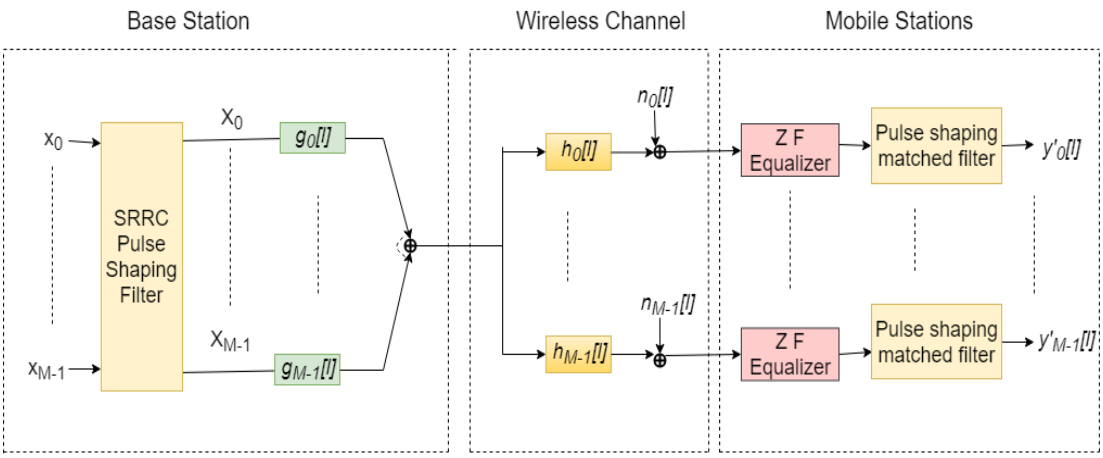

Figure 3.1: TR SIMO System

The mixed signal $S[k]$ is then sent to all the receivers through the rich multipath

environment. At the m^{th} mobile station, the received signal Y_m is

$$Y_m[k] = \underbrace{(h_m \star g_m)[L-1]X_j[k-(L-1)]}_{\text{Desired Signal}} + \underbrace{\sum_{l=0, l\neq L-1}^{2L-2} (h_m \star g_m)[l]X_m[k-l]}_{\text{ISI from own antenna}} + \underbrace{\sum_{i=0, i\neq m}^{M-1} \sum_{l=0}^{2L-2} (h_m \star g_i)[l]X_i[k-l]}_{\text{Inter Antenna Interference}} + \underbrace{n_m[k]}_{\text{noise}} \tag{3.6}$$

The first term in eqn.(3.6) is the desired signal as its coefficient $(h_m \star g_m)[L-1]$ is the tap with the highest energy which is

$$(h_m \star g_m)[L-1] = \frac{\sum_{l=0}^{L-1} |h_m[l]|^2}{\sum_{i=0}^{L-1} |h_m[i]|^2} = 1 \tag{3.7}$$

The second term is the ISI, the third term is the IUI and the last term is the noise. This signal Y_m is then passed through the matched pulse shaping filter and the desired symbol is sampled.

3.1.3 Simulation Results

In this subsection we discuss the simulation results for the case of TR SIMO described in Section 3.1. We consider a symbol rate of 200 Msps, which corresponds to a bandwidth of 200 MHz keeping in mind that we are interested in ultra wideband channels. Simulations are run for a total of 10^6 symbols assuming that the channel remains stationary for every 100 symbols.

From the above BER curve simulated for 2x1 SIMO TR system, we can see that the BER performance is very poor when there is only one transmit antenna. We vary the number of channel taps L and plot the BER. the observation is that as the number of channel taps increase, the BER performance improves. This because of the fact that as the number of channel taps increases, more and more energy is concentrated at the central tap of the equivalent CIR of the system after TR. As a result, the $(L-1)$ taps to the left and right of the central tap decreases in energy as the number of channel taps L

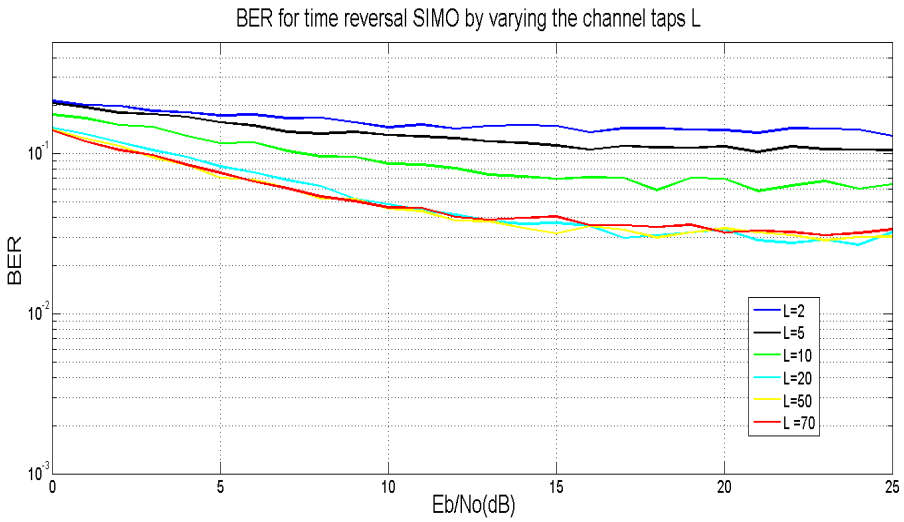

Figure 3.2: BER performance of 2x1 TR SIMO with varying channel taps L

increases and contributes to smaller cumulative interference.

3.2 TR MIMO Downlink Communication

In the previous section we looked at the performance of TR SIMO system. In this section we will analyze the performance gain due to transmit diversity achieved in TR-MIMO system compared to that of TR-SIMO system. We will also study the BER improvement achieved by using a Zero Forcing(ZF) Equalizer at the receiver after TR processing. The implementation of the TR MIMO system is adapted from MIMO-TR-UWB System described in Nguyen *et al.* (2009). In this system we consider N transmit antennas fixed to a base station and M receive antennas each attached to a mobile station.

3.2.1 Channel Model

The channel model is exactly similar to the one described in the previous section for the TR SIMO case. However, this being a MIMO system, there are now KxM realizations between the transmit and receive sides. As before, we assume an L-tap channel model with Rayleigh fading taps which are independent of each other. The CIR between trans-

mit antenna k and receive antenna m in discrete time form is

$$h_{m,k} = [h_{m,k}[0], h_{m,k}[2], ..., h_{m,k}[L-1]]^T \tag{3.8}$$

3.2.2 System Model

In the TR-MIMO case, several streams of data are transmitted over several transmit antennas. The data to be transmitted is first pulse shaped by pulse shaping SRRC filter after upsampling by a factor D to suppress ISI. X_m denotes the data to be transmitted to the m^{th} receiver for all $m \in [0, \boldsymbol{M}-1]$ after pulse shaping. Not that X_m includes the scale factor $\frac{1}{\sqrt{K}}$ for total energy constraint. After pulse shaping, all the signals to different receivers are mixed to form signal S_k at transmitter k for all $k \in [0, K-1]$ as follows.

$$S_k[i] = \sum_{m=0}^{M-1} (X_m \star g_{m,k})[i], \tag{3.9}$$

where

$$g_{m,k}[l] = \frac{h^*_{m,k}[L-1-l]}{\sum\limits_{i=0}^{L-1} |h_{m,k}[i]|^2} \tag{3.10}$$

At the receive side, Y_m is the signal received at the m^{th} mobile station antenna. Y_m can be written as

$$Y_m[i] = \sum_{k=0}^{K-1} (h_{m,k} \star S_k)[i] + n_m[i] \tag{3.11}$$

Upon expanding the RHS of the above expression in eqn.(3.11)

$$\begin{aligned} Y_m[i] = & \underbrace{\sum_{k=0}^{K-1} (h_{m,k} \star g_{m,k})[L-1] X_m[i-(L-1)]}_{\text{Desired Signal}} + \underbrace{\sum_{k=0}^{K-1} \sum_{l=0, l\neq L-1}^{2L-2} (h_{m,k} \star g_{m,k})[l] X_m[i-l]}_{\text{ISI}} \\ & + \underbrace{\sum_{k=0}^{K-1} \sum_{j=0, j\neq m}^{M-1} \sum_{l=0}^{2L-2} (h_{m,k} \star g_{j,k})[l] X_j[i-l]}_{\text{Multi User Interference}} + \underbrace{n_m[i]}_{\text{noise}} \end{aligned} \tag{3.12}$$

The first term of (3.12) is the desired symbol, second term is the ISI, third term is the Multi User Interference (MUI) and last term is the noise. The coefficient of the

desired symbol term is

$$\sum_{k=0}^{K-1}(h_{m,k} \star g_{m,k})[L-1] = \sum_{k=0}^{K-1} \frac{\sum_{l=0}^{L-1} |h_{m,k}[l]|^2}{\sum_{i=0}^{L-1} |h_m(i)|^2} = \sum_{k=0}^{K-1} 1 = K \tag{3.13}$$

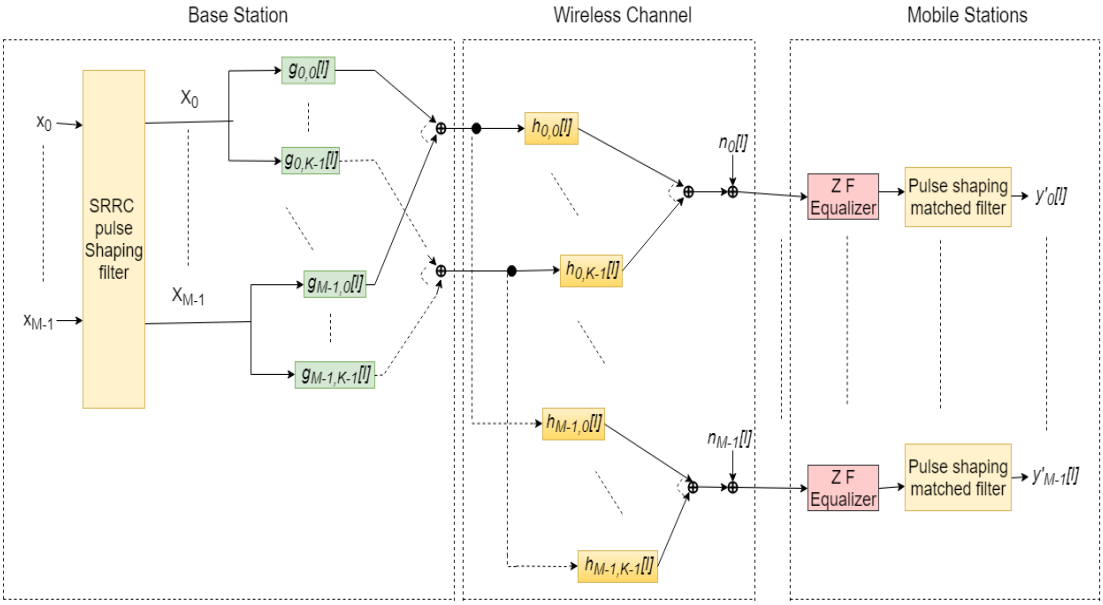

Figure 3.3: TR MIMO System

As a result the desired signal is the transmitted signal boosted up by a factor K which is the transmit diversity gain term. Despite the transmit diversity gain, the desired signal suffers from an increased interference (both ISI and MUI). We will analyze the net effect of degradation due to interference and increase diversty gain in the upcoming subsection where we present the BER performance for TR MIMO system.

The received signal Y_m is then sent through the matched pulse shaping filter and desired symbol is sampled.

3.2.3 Implementation of TR-MIMO - Matrix Representation

In case of MIMO system, the complexity increases depending on the number of transmit and receive antennas. This makes implementation of the system during simulation very tedious as a lot of convolution operations need to be performed. One way to reduce this complexity is by performing convolution in terms of matrix multiplication. Of

course, this would mean that the system should have large memory. This ensures that the time involved in execution of the program is small. In this subsection, we present the implementation of the above described TR-MIMO system in terms of matrix operations.

As defined previously in eqn.(3.8), the CIR between the transmit antenna k and the receive antenna m in discrete time is $h_{m,k}$. We define the vector $\mathbf{h}_{m,k}$ as the CIR between transmit antenna k and receive antenna m in reverse order

$$\mathbf{h}_{m,k} = [h_{m,k}[L-1], h_{m,k}[L-2], ..., h_{m,k}[0]]^T \tag{3.14}$$

The entire CIR matrix between the transmitter and receiver is

$$\mathbf{H} = \begin{bmatrix} \mathbf{h}_{0,0} & \mathbf{h}_{1,0} & \cdots & \mathbf{h}_{M-1,0} \\ \mathbf{h}_{0,1} & \mathbf{h}_{1,1} & \cdots & \mathbf{h}_{M-1,1} \\ \vdots & \vdots & \ddots & \vdots \\ \mathbf{h}_{0,K-1} & \mathbf{h}_{1,K-1} & \cdots & \mathbf{h}_{M-1,K-1} \end{bmatrix}^T, \tag{3.15}$$

with dimension MxKL.

In TR-MIMO, the CIR of all channels $h_{m,k}$ are known at the transmitter side. The normalized, time-reversed version of these CIRs are used to filter the transmit data. We construct a filtering matrix based on the time reversed version of the CIRs. This matrix is an KLx$M(2L-1)$ matrix given by

$$\mathbf{G} = \begin{bmatrix} \mathbf{G}_{0,0} & \mathbf{G}_{1,0} & \cdots & \mathbf{G}_{M-1,0} \\ \mathbf{G}_{0,1} & \mathbf{G}_{1,1} & \cdots & \mathbf{G}_{M-1,1} \\ \vdots & \vdots & \ddots & \vdots \\ \mathbf{G}_{0,K-1} & \mathbf{G}_{1,K-1} & \cdots & \mathbf{G}_{M-1,K-1} \end{bmatrix}, \tag{3.16}$$

where each submatrix $G_{m,k}$ is an Lx$(2L-1)$ Toeplitz matrix defined by

$$\mathbf{G}_{m,k} = \begin{bmatrix} g_{m,k}[L-1] & \cdots & g_{m,k}[0] & 0 & \cdots & 0 \\ 0 & g_{m,k}[L-1] & \cdots & g_{m,k}[0] & \cdots & 0 \\ \vdots & \ddots & \ddots & \ddots & \ddots & \vdots \\ 0 & \cdots & 0 & g_{m,k}[L-1] & \cdots & g_{m,k}[0] \end{bmatrix} \tag{3.17}$$

This is equivalent to

$$\mathbf{G}_{m,k} = \frac{1}{\sum_{i=0}^{L-1} |h_{m,k}[i]|^2} \begin{bmatrix} h_{m,k}[0] & \cdots & h_{m,k}[L-1] & 0 & \cdots & 0 \\ 0 & h_{m,k}[0] & \cdots & h_{m,k}[L-1] & \cdots & 0 \\ \vdots & \ddots & \ddots & \ddots & \ddots & \vdots \\ 0 & \cdots & 0 & h_{m,k}[0] & \cdots & h_{m,k}[L-1] \end{bmatrix}. \tag{3.18}$$

The equivalent channel response is $\hat{\mathbf{H}} = \mathbf{HG}$ which has dimension Nx$N(2L-1)$.

$$\hat{\mathbf{H}} = \begin{bmatrix} \hat{\mathbf{h}}_{0,0} & \hat{\mathbf{h}}_{1,0} & \cdots & \hat{\mathbf{h}}_{M-1,0} \\ \hat{\mathbf{h}}_{0,1} & \hat{\mathbf{h}}_{1,1} & \cdots & \hat{\mathbf{h}}_{M-1,1} \\ \vdots & \vdots & \ddots & \vdots \\ \hat{\mathbf{h}}_{0,M-1} & \hat{\mathbf{h}}_{1,M-1} & \cdots & \hat{\mathbf{h}}_{M-1,M-1} \end{bmatrix}^T. \tag{3.19}$$

Each element $\hat{\mathbf{h}}_{i,j}$ is an $(2L-1)$x1 auto-correlation or cross-correlation vector. The peak value of the auto-correlation is at $(L-1)$-th index.

Let us consider a block of N+$2L$-1 symbols of the transmit data to be sent to the m^{th} receiver antenna. We assume that channel does not change within this block. This block of data can be represented by an $(2L-1)$xN matrix

$$\mathbf{X}_m = \begin{bmatrix} x_m[i-2L+2] & x_m[i-2L+3] & \cdots & x_m[i-2L+N-1] \\ \vdots & \vdots & \cdots & \vdots \\ x_m[i-1] & x_m[i] & \cdots & x_m[i+N-2] \\ x_m[i] & x_m[i+1] & \cdots & x_m[i+N-1] \end{bmatrix}. \tag{3.20}$$

The entire transmit signal matrix is

$$\mathbf{X} = \frac{1}{\sqrt{K}} [\mathbf{X}_0, \mathbf{X}_1, ..., \mathbf{X}_{M-1}]^T, \tag{3.21}$$

with the dimension $M(2L-1)$xN. The scale factor $1/\sqrt{K}$ keeps the total transmit power of the signal as the same as in the SISO case. The additive Gaussian noise at the m^{th} receiver antenna is a Nx1 vector

$$\mathbf{n}_m = [n_m[i], n_m[i+1], ..., n_m[i+N-1]]^T, \tag{3.22}$$

and the entire noise matrix is an MxN matrix

$$\mathbf{n} = [\mathbf{n}_0, \mathbf{n}_1, ..., \mathbf{n}_{M-1}]^T, \tag{3.23}$$

The matrix of the received signal with TR pre-filtering is

$$\mathbf{Y} = \mathbf{HGX} + \mathbf{n} \tag{3.24}$$

$$= \hat{\mathbf{H}}\mathbf{X} + \mathbf{n} \tag{3.25}$$

where each row of the received matrix $\mathbf{Y}$ is

$$\mathbf{y}_m = [y_m[i], y_m[i+1], ..., y_m[i+N-1]], m = 0, 1, ..., M-1. \tag{3.26}$$

Substituting eqns.(3.15),(3.16) and (3.20) into eqn.(3.24), the received signal at the m^{th} receiver can be expressed by

$$\mathbf{y}_m = \sum_{j=0}^{K-1} \mathbf{h}_{m,j}^T \hat{\mathbf{H}}_{m,j} \mathbf{X}_m + \sum_{j=0}^{K-1} \sum_{i=0, i\neq m}^{M-1} \mathbf{h}_{m,j}^T \hat{\mathbf{H}}_{i,j} \mathbf{X}_i + \mathbf{n}_m^T. \tag{3.27}$$

The first part of the received signal is the desired data stream with the summation of the auto-correlation of K channels. The second part is the interference from other streams. In the second part, the equivalent channel is the cross-correlation of channels, which is generally small in comparison to the former.

3.2.4 ZF equalizer at the transmitter

The performance of the TR MIMO system can be further improved by using a ZF equalizer at each receiver. One of the advantages of writing and implementing the system in matrix notation is that we have a well-defined equivalent channel matrix whose inverse can be computed for equalizer implementation. From (3.27), the coefficient of the desired signal $\mathbf{X}_m$ is 1x$(2L-1)$ row vector $\mathbf{Heq}_m$ given by

$$\mathbf{Heq}_m = \sum_{j=0}^{K-1} \mathbf{h}_{m,j}^T \hat{\mathbf{H}}_{m,j} \tag{3.28}$$

At each receiver, the ZF equalizer can be implemented to get the desired signal $\hat{\mathbf{y}}_m$

given by

$$\hat{\mathbf{y}}_m = (\mathbf{Heq}_m^H \mathbf{Heq}_m)^{-1} \mathbf{Heq}_m^H \mathbf{y}_m \tag{3.29}$$

The equalizer needed will be for a $(2L-1)$ tap channel. As a result, the complexity of the equalizer required at the receiver is almost doubled. Another requirement for implementing an equalizer at the receiver m is that the receiver should be aware of the CSI from all K transmit antennas. This increases the complexity of the receiver immensely.

To overcome the first problem, we can take advantage of the focussing effect of the TR signal. We are aware of the fact that most of the energy of the equivalent channel is centred around the central taps. So, we can pick only L_{eff} central taps of the equivalent channel and design the equalizer with this as the channel response. This reduces the complexity of the receiver. We describe the results of using ZF equalizer by varying L_{eff} in the next subsection, where we present the simulation results.

3.2.5 Simulation Results

In this subsection we discuss the simulation results for the case of TR MIMO described in Section 3.2. We consider a symbol rate of 200 Msps, which corresponds to a bandwidth of 200 MHz keeping in mind that we are interested in ultra wideband channels. We run our simulations for a total of 10^6 symbols assuming that the channel remains stationary for every 100 symbols.

Figs. 3.4(a),(b) and (c) provide a comprehensive picture for analysis of the simulation results obtained in this section. Theoretic BER for BSPK in AWGN is also plotted for reference.

- "sim BER TR" denotes simulation BER for TR-MIMO system without equalization.
- "sim BER TR ZF" denotes simulation BER for TR-MIMO system followed by ZF Equalizer.

For the plots in Figure 3.4, the $x_k[l]$ is upsampled at the transmitter by a factor of $D = 3$ before pulse shaping as mentioned in Section 3.2.2.

Insights:

1. From Figures 3.4(a) and 3.4(b) we can see that the BER performance degrades as

the number of receiver antennas M increases keeping the number of transmit antennas K constant. This is because of increase in the multiuser interference as the number of users increases.
2. From Figures 3.4(b) and 3.4(c) we can see that the BER performance improves as the number of transmit antennas K increases keeping the number of receive antenna M constant. This is due to the increase in transmit diversity gain as the number of transmitters increase.
3. ZF equalizer based on all $(2L-1)$ taps of the equivalent CIR is able to improve the performance only by a small amount.

When compared to the simulation result for TR-SIMO case in Subsection 3.1.3, we can clearly see that TR MIMO performs better in terms of BER, inspite of an increased number of interference terms. This is because of the substantial transmit diversity benefit achieved in TR-MIMO case, which is able to compensate the degradation due to increased interference. The net effect is positive, which results in better BER performance. To put this in terms of numbers, let K be the number of transmit antennas and M be the number of receive antennas in TR-MIMO case.

For TR SIMO, $K = 1$, as a result the power of the central term in equivalent CIR is 1. There are $(M-1)$ multiuser interference terms corresponding to the M receivers.

For TR MIMO case, the power of the central term in equivalent channel response is K due to the transmit diversity benefit by a factor of K. But there are $(M-1)K$ interference terms.

From the above simulation, it is seen that the net effect of diversity gain of K and interference form $(M-1)K$ terms is more positive than that of diversity gain of 1 and interference form $(M-1)$ terms.

There are a few issues with implementation of TR-MIMO system at the transmitter described in this Chapter. Firstly, upsampling the signal before pulse shaping at the transmitter increases overhead/bandwidth considerably. Secondly, for implementing an equalizer at the receiver, it should be aware of the CSI from all K transmit antennas. This means that CSI should be available at both the transmitter and the receiver. In the next Chapter we try to overcome these challenges by implementing TR-MIMO at the receiver.

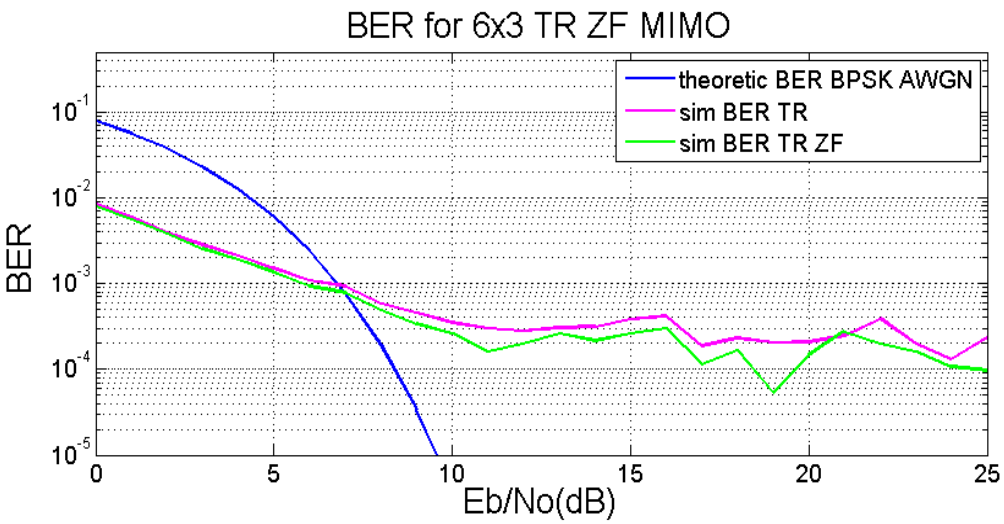

(a) 6x3 TR ZF BER

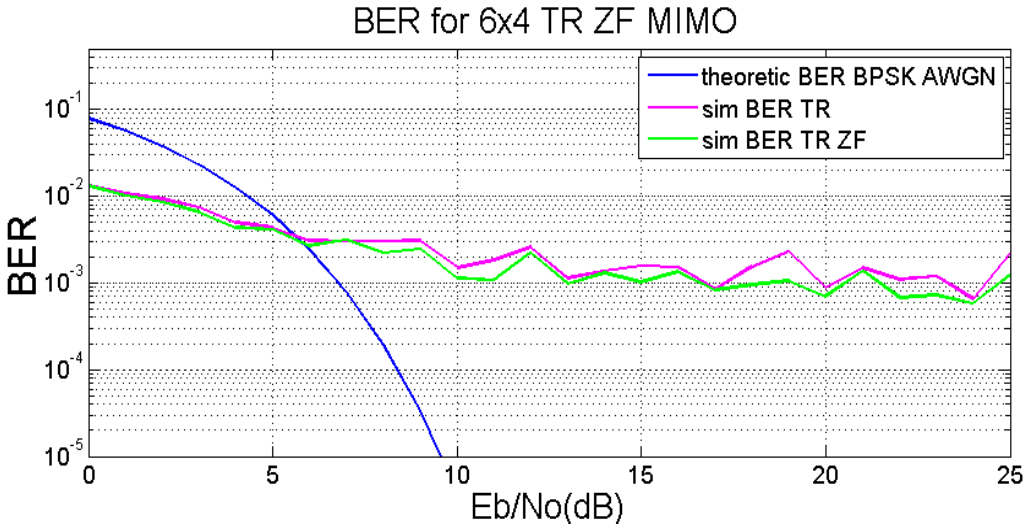

(b) 6x4 TR ZF BER

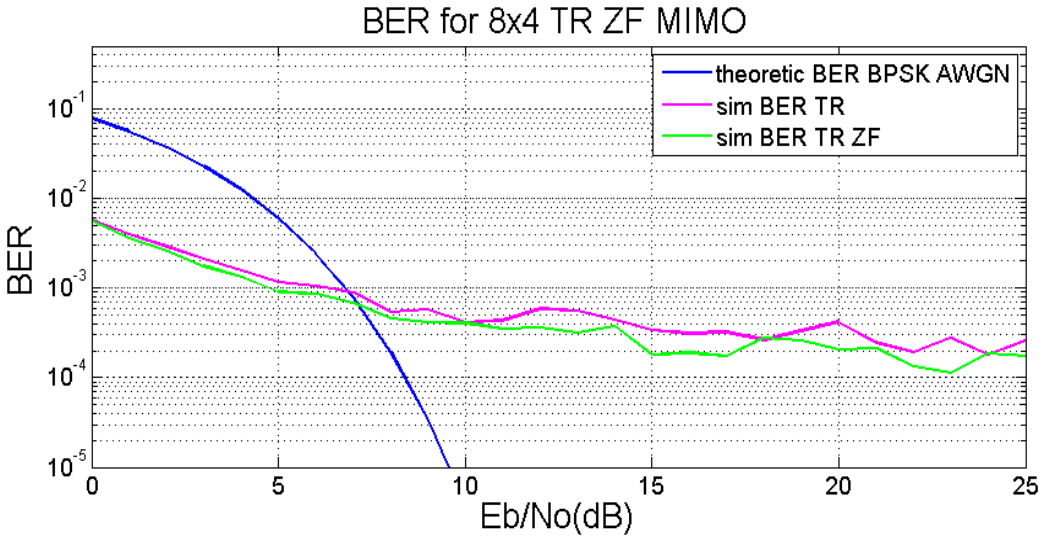

(c) 8x4 TR ZF BER

Figure 3.4: BER performance of TR MIMO for different transmitter & receiver configurations for 20 tap channel. TR ZF stands for ZF equalization after TR.

CHAPTER 4

TR processing at Receiver: Combining OFDM and TR

In the previous Chapter, we studied TR processing at the transmitter ie., we assumed the transmitter is present at the base station and all the TR processing is done at the base station. We learnt that TR-MIMO yields better results compared to TR SIMO communication system due to its superior transmit diversity gain which overcomes the degradation due to augmented interference and noise. However, there are a few issues with the implementation of TR MIMO system described in the previous Chapter. Firstly, there is a substantial overhead due to upsampling of the data before pulse shaping at the transmitter to reduce the ISI. Secondly, implementation of the equalizer at the receiver requires the knowledge of CSI from all the transmitters, which requires implementation of complex receivers. One good solution to the second problem is to do **TR processing at the receiver**. It would also be good if we could somehow be able to get rid of the upsampling overhead. Orthogonal Frequency-Division Multiplexing (OFDM) presents an attractive option to overcome this problem of upsampling as the different symbols in an OFDM block are sent over different subcarriers that are orthogonal to each other. As a result, the need for upsampling is eliminated. This idea led to exploring the applications of TR and OFDM for MIMO communications. There have been some work done on this idea by Farhang *et al.* (2016). In Aminjavaheri *et al.* (2017), an OFDM without CP based solution for Massive MIMO applications is presented, where Cyclic Prefix (CP) has been removed to increase the spectral efficiency and time reversal is employed to deal with interference. Being a massive MIMO system, the results presented show that the asymptotic achievable rate or capacity of the system can be increased (without saturation) by increasing the number of base station antennas.

Taking inspiration from Aminjavaheri *et al.* (2017), we will investigate the BER performance of the MIMO OFDM system without CP and use TR to counter the effects of ISI and Inter Block Interference (IBI). We are specifically interested in the case where the number of base station antennas are small compared to Massive MIMO where the number of antennas can be of the order of 100s. We also present a Decision Feedback based Interference Cancellation (DFIC) scheme to improve the BER performance after

TR processing. A Zero Forcing equalizer with lower complexity can then be used to further improve the performance. Based on these modifications,we present the analytical expressions and simulation results for our OFDM (without CP) TR system and compare the performance of the system after each post processing steps. We also compare the BER performance with that of MIMO OFDM with CP. Finally, we present insights gained from our implementation.

4.1 OFDM without CP followed by Time Reversal

In this section, we present a MIMO system based on OFDM without CP. OFDM is similar to Frequency-division Multiplexing (FDM) but the different carriers are closely spaced enabled by the choice of orthogonal carriers. OFDM handles frequency selectivity by dividing a frequency selective channel into smaller flat fading channels called as sub-carriers and each sub-carrier modulates different transmit baseband symbols as in FDM. The addition of Cyclic Prefix (CP) at the beginning of an OFDM symbol alleviates the effects of multipath channel and helps in avoiding ISI between adjacent OFDM symbols .

However, in our system, we are interested in OFDM without CP or with insufficient CP. The reason for removing CP is, it causes high overhead in case of multipath channels with large delay spread compared to the time resolvability window. This is for the case where the delay spread of the multipath channel is greater that 50 times $T_s = 1/Bandwidth$ of the system. Consequently, the number of channel taps will also be large (>50 in this case).

We consider the case of uplink transmission, assuming that base station will have enough resources to perform TR and other post processing techniques. The MIMO system consists of K transmit mobile terminals and M receive antennas which are fixed to the base station.

4.1.1 Channel Model

The channel model is exactly similar to the one described in the previous Chapter for the TR MIMO case. As before, we assume an L-tap channel model with Rayleigh

fading taps which are independent of each other. The CIR between transmit antenna k and receive antenna m in discrete time form is

$$h_{m,k} = [h_{m,k}[0], h_{m,k}[2], ..., h_{m,k}[L-1]]^T \tag{4.1}$$

4.1.2 System Model

We consider a discrete-time model for our analysis which is followed in Aminjavaheri *et al.* (2017). Let $x_k[l]$ represent the transmit signal of the k^{th} mobile terminal in discrete time. Thus, the received signal at the m^{th} receiver antenna can be obtained as

$$y_m[l] = \sum_{k=0}^{K-1} x_k[l] \star h_{m,k}[l] + n_m[l], \tag{4.2}$$

where $n_m[l]$ is the complex additive white Gaussian noise at the input of m^{th} receiver antenna.

In this Chapter we assume OFDM modulation is used for data transmission with the total number of N subcarriers. For our case of OFDM without CP, we don't insert CP bits in between the successive OFDM blocks. Therefore, the i^{th} OFDM block of transmitter k can be obtained as

$$\mathbf{x}_{k,i} = \mathbf{F}_N^H \mathbf{d}_{k,i}, \tag{4.3}$$

where $\mathbf{F}_N$ is the N-point normalized Discrete Fourier Transform (DFT) matrix and $\mathbf{d}_{k,i} = [d_{k,i}[0], d_{k,i}[1], ..., d_{k,i}[N-1]^T$ is the transmit data vector of terminal k on symbol time index i.

We can write the expression of received block $\mathbf{y}_{m,i} = [y_m[iN], y_m[iN+1], ..., y_m[iN+N-1]]^T$ at the receiver m at time index i in terms of channel matrices $\mathbf{H}_{m,k}^{(i,i-1)}$ and $\mathbf{H}_{m,k}^{(i,i)}$.

These are NxN convolution matrices defined below.

$$\mathbf{H}_{m,k}^{(i,i-1)} = \begin{bmatrix} 0 & \cdots & h_{m,k}[L-1] & h_{m,k}[L-2] & \cdots & h_{m,k}[1] \\ 0 & \cdots & 0 & h_{m,k}[L-1] & \cdots & h_{m,k}[2] \\ \vdots & \ddots & \vdots & \vdots & \ddots & \vdots \\ 0 & \cdots & \cdots & \cdots & \cdots & h_{m,k}[L-1] \\ 0 & \cdots & \cdots & \cdots & \cdots & 0 \\ \vdots & \vdots & \vdots & \vdots & \ddots & \vdots \\ 0 & \cdots & \cdots & \cdots & \cdots & 0 \end{bmatrix} \tag{4.4}$$

,

$$\mathbf{H}_{m,k}^{(i,i)} = \begin{bmatrix} h_{m,k}[0] & 0 & 0 & \cdots & 0 \\ h_{m,k}[1] & h_{m,k}[0] & 0 & \cdots & 0 \\ \vdots & \vdots & \vdots & \ddots & \vdots \\ h_{m,k}[L-1] & h_{m,k}[L-2] & h_{m,k}[L-3] & \cdots & 0 \\ 0 & h_{m,k}[L-1] & h_{m,k}[L-2] & \cdots & 0 \\ \vdots & \vdots & \vdots & \ddots & \vdots \\ 0 & 0 & 0 & \cdots & h_{m,k}[0] \end{bmatrix}, \tag{4.5}$$

Based on the definitions in eqns.(4.3),(4.4) and (4.5), eqn.(4.2) can be rewritten in matrix form as

$$\mathbf{y}_{m,i} = \sum_{k=0}^{K-1} \mathbf{H}_{m,k}^{(i,i-1)} \mathbf{x}_{k,i-1} + \mathbf{H}_{m,k}^{(i,i)} \mathbf{x}_{k,i} + \mathbf{n}_{m,i}. \tag{4.6}$$

The matrices $\mathbf{H}_{m,k}^{(i,i-1)}$ and $\mathbf{H}_{m,k}^{(i,i)}$, when multiplied to the vectors $\mathbf{x}_{k,i-1}$ and $\mathbf{x}_{k,i}$, create the tail of the block i-1 overlapping with L-1 symbols in the beginning of the block i and the channel affected block i, respectively. The vector $\mathbf{n}_{m,i}$ includes N samples of the AWGN signal $n_m[l]$ at the position of block i.

At the base station, for a given transmitter mobile terminal, say k, the received signals are first pre-filtered with the time-reversed versions of the Channel Impulse Response (CIRs) between that terminal and the corresponding base station receiver antennas. Then, the resulting signals are combined with each other. Using eqn.(4.2), this

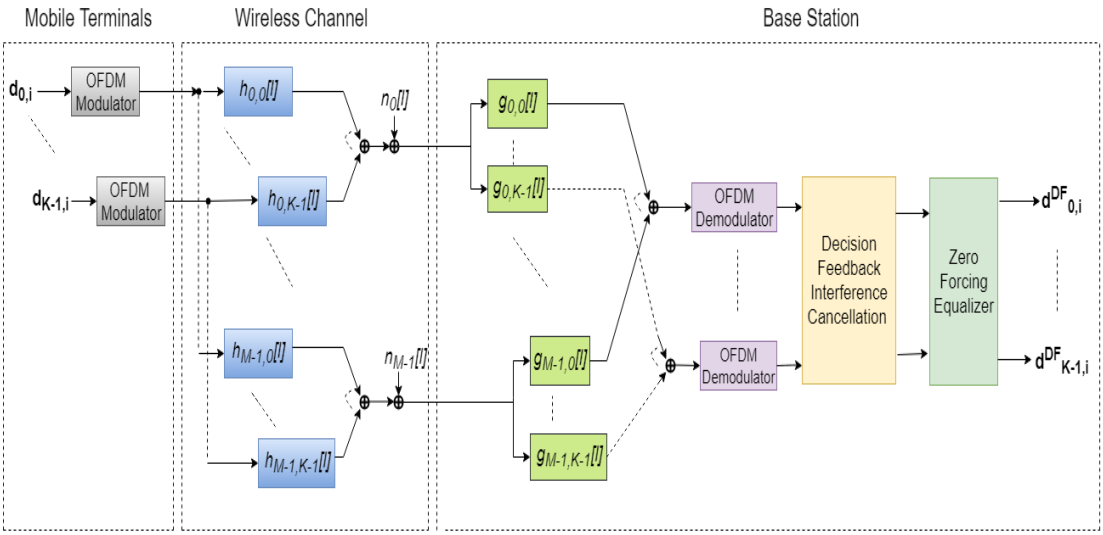

Figure 4.1: OFDM without CP Time Reversal System

procedure can be mathematically written as

$$y_k^{TR}[l] = \sum_{m=0}^{M-1} y_m[l] \star g_{m,k}[l] = \sum_{j=0}^{K-1} x_j[l] \star u_{kj}[l] + n_k^{TR}[l], \tag{4.7}$$

where

$$u_{kj}[l] \triangleq \sum_{m=0}^{M-1} h_{m,j}[l] \star g_{m,k}[l], \tag{4.8}$$

and

$$g_{m,k}(l) = \frac{h_{m,k}^*(L-1-l)}{\sum_{i=0}^{L-1} |h_{m,k}(i)|^2}. \tag{4.9}$$

Here $u_{kj}[l]$ is the equivalent composite CIR after TR operation. In particular, $u_{kj}[l]$ for $j \neq k$, is the cross-talk CIR between the transmitters k and j, and $u_{kk}[l]$ is the time reversal equivalent CIR of the transmitter k. $n_k^{TR}[l] \triangleq \sum_{m=0}^{M-1} n_m[l] \star g_{m,k}[l]$ is the noise contribution after TR operation.

We can write the expression of i^{th} block of the signal $y_k^{TR}[l]$ as a Nx1 vector $\mathbf{y}_{k,i}^{TR} = [y_k^{TR}[iN], y_k^{TR}[iN+1], ..., y_k^{TR}[iN+N-1]]^T$ in terms of equivalent channel matrices $\mathbf{U}_{kj}^{(i,i-1)}$,$\mathbf{U}_{kj}^{(i,i)}$ and $\mathbf{U}_{kj}^{(i,i+1)}$. These are NxN convolution matrices defined below.

$$\mathbf{U}_{kj}^{(i,i-1)} = \begin{bmatrix} 0 & \cdots & u_{kj}[2L-2] & u_{k,j}[2L-3] & \cdots & u_{kj}[L] \\ 0 & \cdots & 0 & u_{kj}[2L-2] & \cdots & u_{kj}[L+1] \\ \vdots & \ddots & \vdots & \vdots & \ddots & \vdots \\ 0 & \cdots & \cdots & \cdots & \cdots & u_{kj}[2L-2] \\ 0 & \cdots & \cdots & \cdots & \cdots & 0 \\ \vdots & \vdots & \vdots & \vdots & \ddots & \vdots \\ 0 & \cdots & \cdots & \cdots & \cdots & 0 \end{bmatrix} \tag{4.10}$$

,

$$\mathbf{U}_{kj}^{(i,i)} = \begin{bmatrix} u_{kj}[L-1] & u_{kj}[L-2] & \cdots & u_{kj}[1] & u_{kj}[0] & 0 & \cdots & 0 \\ u_{kj}[L] & u_{kj}[L-1] & \cdots & u_{kj}[2] & u_{kj}[1] & u_{kj}[0] & \cdots & 0 \\ \vdots & \vdots & \ddots & \vdots & \vdots & \vdots & \ddots & \vdots \\ u_{kj}[2L-2] & u_{kj}[2L-3] & \cdots & u_{kj}[L] & u_{kj}[L-1] & u_{kj}[L-2] & \cdots & 0 \\ 0 & u_{kj}[2L-2] & \cdots & u_{kj}[L+1] & u_{kj}[L] & u_{kj}[L-1] & \cdots & 0 \\ \vdots & \vdots & \ddots & \vdots & \vdots & \vdots & \ddots & \vdots \\ 0 & 0 & \cdots & 0 & 0 & 0 & \cdots & u_{kj}[L-1] \end{bmatrix} \tag{4.11}$$

,

$$\mathbf{U}_{kj}^{(i,i+1)} = \begin{bmatrix} 0 & 0 & \cdots & 0 & 0 & \cdots & 0 \\ \vdots & \vdots & \ddots & \vdots & \vdots & \ddots & \vdots \\ u_{kj}[0] & 0 & \cdots & 0 & 0 & \cdots & 0 \\ u_{kj}[1] & u_{kj}[0] & \cdots & 0 & 0 & \cdots & 0 \\ \vdots & \vdots & \ddots & \vdots & \vdots & \ddots & \vdots \\ u_{kj}[L-3] & u_{kj}[L-4] & \cdots & u_{kj}[0] & 0 & \cdots & 0 \\ u_{kj}[L-2] & u_{kj}[L-3] & \cdots & u_{kj}[1] & u_{kj}[0] & \cdots & 0 \end{bmatrix}. \tag{4.12}$$

Based on the definitions in eqns.(4.10),(4.11) and (4.12), eqn.(4.7) can be rewritten

in matrix form as

$$\mathbf{y}_{k,i}^{TR} = \sum_{j=0}^{K-1} (\mathbf{U}_{kj}^{(i,i-1)} \mathbf{x}_{j,i-1} + \mathbf{U}_{kj}^{(i,i)} \mathbf{x}_{j,i} + \mathbf{U}_{kj}^{(i,i+1)} \mathbf{x}_{j,i+1}) + \mathbf{n}_{k,i}^{TR}, \tag{4.13}$$

where the vector $\mathbf{n}_{k,i}^{TR}$ contains N samples of the AWGN signal $n_k^{TR}[l]$ at the position of the block i. The matrices $\mathbf{U}_{kj}^{(i,i-1)}$,$\mathbf{U}_{kj}^{(i,i)}$ and $\mathbf{U}_{kj}^{(i,i+1)}$ are convolution matrices comprising the Inter Block Interference (IBI) components due to the tail of the block i-1, the ISI components within the block i and the IBI components originating from the beginning of the block i+1, respectively.

We then send the signal $\mathbf{y}_{k,i}^{TR}$ through a DFT block to recover the bits sent over the different subcarriers. Mathematically, this can be written as

$$\begin{aligned} \bar{\mathbf{y}}_{k,i}^{TR} &= \mathbf{F}_N \Bigg(\sum_{j=0}^{K-1} \Big(\mathbf{U}_{kj}^{(i,i-1)} \mathbf{x}_{j,i-1} + \mathbf{U}_{kj}^{(i,i)} \mathbf{x}_{j,i} + \mathbf{U}_{kj}^{(i,i+1)} \mathbf{x}_{j,i+1} \Big) + \mathbf{n}_{k,i}^{TR} \Bigg) \\ &= \sum_{j=0}^{K-1} \Big(\bar{\mathbf{U}}_{kj}^{(i,i-1)} \mathbf{d}_{j,i-1} + \bar{\mathbf{U}}_{kj}^{(i,i)} \mathbf{d}_{j,i} + \bar{\mathbf{U}}_{kj}^{(i,i+1)} \mathbf{d}_{j,i+1} \Big) + \bar{\mathbf{n}}_{k,i}^{TR}, \end{aligned} \tag{4.14}$$

where $\bar{\mathbf{U}}_{kj}^{(i,i-1)} = \mathbf{F}_N \mathbf{U}_{kj}^{(i,i-1)} \mathbf{F}_N^H$, $\bar{\mathbf{U}}_{k,j}^{(i,i)} = \mathbf{F}_N \mathbf{U}_{kj}^{(i,i)} \mathbf{F}_N^H$, $\bar{\mathbf{U}}_{kj}^{(i,i+1)} = \mathbf{F}_N \mathbf{U}_{kj}^{(i,i+1)} \mathbf{F}_N^H$ and $\bar{\mathbf{n}}_{k,i}^{TR} = \mathbf{F}_N \mathbf{n}_{k,i}^{TR} \mathbf{F}_N^H$.

In order to understand the above equation, we need to write down the expression for the p^{th} element of the recovered data vector $\bar{\mathbf{y}}_{k,i}^{TR}$. Let $\bar{y}_{k,i}^{TR}[p]$ be the p^{th} element of vector $\bar{\mathbf{y}}_{k,i}^{TR}$. Also, let $U_{kj,pq}^{(i,i-1)}$, $U_{kj,pq}^{(i,i)}$ and $U_{kj,pq}^{(i,i+1)}$ be the element at the p^{th} row and q^{th} column of the matrices $\bar{\mathbf{U}}_{kj}^{(i,i-1)}$, $\bar{\mathbf{U}}_{k,j}^{(i,i)}$ and $\bar{\mathbf{U}}_{kj}^{(i,i+1)}$ respectively. Then $\bar{y}_{k,i}^{TR}[p]$ can be written as

$$\begin{aligned} \bar{y}_{k,i}^{TR}[p] = \underbrace{U_{kk,pp}^{(i,i)} d_{k,i}[p]}_{\text{Desired Signal}} + \underbrace{\sum_{q=0, q\neq p}^{N-1} U_{kk,pq}^{(i,i)} d_{k,i}[q]}_{\text{Intra Block Interference}} + \underbrace{\sum_{q=0}^{N-1} \Big(U_{kk,pq}^{(i,i-1)} d_{k,i-1}[q] + U_{kk,pq}^{(i,i+1)} d_{k,i+1}[q] \Big)}_{\text{Inter Block Interference}} \\ + \underbrace{\sum_{j=0, j\neq k}^{K-1} \sum_{q=0}^{N-1} \Big(U_{kj,pq}^{(i,i-1)} d_{j,i-1}[q] + U_{kj,pq}^{(i,i)} d_{j,i}[q] + U_{kj,pq}^{(i,i+1)} d_{j,i+1}[q] \Big)}_{\text{Multi User Interference}} + \underbrace{\bar{n}_{k,i}^{TR}[p]}_{\text{Noise}}. \end{aligned} \tag{4.15}$$

From the above eqn.(4.15), we can see that although the desired term has high energy coefficient, it still suffers from interference from the symbols in the current block i, Inter

Block Interference (IBI) from the previous and future blocks. In the next subsection we will try to get rid of Intra Block Interference and Multi User Interference (MUI) terms for the current block i by employing ZF equalizer for a particular subcarrier. We will then try to remove IBI terms from the previous block as well as the interference terms from the past symbols in the current block by using a Decision Feedback based Interference Cancellation (DFIC) mechanism described in the later subsection.

4.1.3 Zero Forcing Post Equalization

The structure of OFDM helps us to design a multiuser equalizer after TR. We consider each subcarrier individually, and apply Zero Forcing (ZF) matrix constraint to eliminate the interference coming from different transmit antennas. To generate the ZF matrix for a given subcarrier p, we reformulate the eqn.(4.15) as follows.

Let $\bar{\mathbf{y}}_i^{TR}[p] = [\bar{y}_{0,i}^{TR}[p], ..., \bar{y}_{K-1,i}^{TR}[p]]^T$ contain the p^th output of the DFT blocks for the different terminals. Similarly, we define the noise vector $\bar{\mathbf{n}}_i^{TR}[p] = [\bar{n}_{0,i}^{TR}[p], ..., \bar{n}_{K-1,i}^{TR}[p]]^T$. To express different interference terms, we construct KxK matrices $\boldsymbol{U}_{pq}^{(i,i-1)}$,$\boldsymbol{U}_{pq}^{(i,i)}$ and $\boldsymbol{U}_{pq}^{(i,i+1)}$ according to $\left[\boldsymbol{U}_{pq}^{(i,i-1)}\right]_{kj} = U_{kj,pq}^{(i,i-1)}$, $\left[\boldsymbol{U}_{pq}^{(i,i)}\right]_{kj} = U_{kj,pq}^{(i,i)}$ and $\left[\boldsymbol{U}_{pq}^{(i,i+1)}\right]_{kj} = U_{kj,pq}^{(i,i+1)}$. Note that $\left[\mathbf{A}\right]_{kj}$ denotes the element at k^{th} row and j^{th} column of matrix $\mathbf{A}$. Following the above definitions, we can rearrange eqn.(4.15) as

$$\bar{\mathbf{y}}_i^{TR}[p] = \boldsymbol{U}_{pp}^{(i,i)}\mathbf{d}_i[p] + \sum_{q=0,q\neq p}^{N-1} \boldsymbol{U}_{pq}^{(i,i)}\mathbf{d}_i[q] + \sum_{q=0}^{N-1} \left(\boldsymbol{U}_{pq}^{(i,i-1)}\mathbf{d}_{i-1}[q] + \boldsymbol{U}_{pq}^{(i,i+1)}\mathbf{d}_{i+1}[q]\right) + \bar{\mathbf{n}}_i^{TR}[p]. \tag{4.16}$$

The term $\boldsymbol{U}_{pp}^{(i,i)}\mathbf{d}_i[p]$ contains the desired signals as well as the interference from i^{th} blocks of different mobile terminals transmitted in the same subcarrier frequency slot p. More specifically, the diagonal elements of $\boldsymbol{U}_{pp}^{(i,i)}$ correspond to the desired signal terms and the off-diagonal elements correspond to the interference terms. The ZF equalizer matrix is the inverse of the matrix $\boldsymbol{U}_{pp}^{(i,i)}$. The recovered data for the p^{th} subcarrier after ZF equalization can be written as

$$\hat{\mathbf{d}}_i[p] = \left(\boldsymbol{U}_{pp}^{(i,i)}\right)^{-1} \bar{\mathbf{y}}_i^{TR}[p]. \tag{4.17}$$

We now describe an easy way to generate the matrix $\boldsymbol{U}_{pp}^{(i,i)}$. Recall that

$$\left[\boldsymbol{U}_{pp}^{(i,i)}\right]_{kj} = U_{kj,pp}^{(i,i)} = \left[\bar{\mathbf{U}}_{k,j}^{(i,i)}\right]_{pp} = \mathbf{f}_p^T \mathbf{U}_{kj}^{(i,i)} \mathbf{f}_p^*, \tag{4.18}$$

where $\mathbf{f}_p$ is the $(p-1)^{th}$ row of the DFT matrix. After some algebraic manipulations $\left[\boldsymbol{U}_{pp}^{(i,i)}\right]_{kj}$ can be found as

$$\left[\boldsymbol{U}_{pp}^{(i,i)}\right]_{kj} = U_{kj,pp}^{(i,i)} = \mathbf{f}_p^T \mathbf{U}_{kj}^{(i,i)} \mathbf{f}_p^* = \frac{1}{N} \sum_{l=0}^{2L-2} \Big(N - |l-(L-1)|\Big) u_{kj}[l] e^{-j\frac{2\pi\left(l-(L-1)\right)p}{N}}. \tag{4.19}$$

Based on the above expression, $\left[\boldsymbol{U}_{pp}^{(i,i)}\right]_{kj}$ is equal to the p^{th} coefficient of the N-point DFT of the signal $u'_{kj} \triangleq \frac{\left(N-|l-(L-1)|\right)}{N} u_{kj}[l] e^{j\frac{2\pi(L-1)p}{N}}$. Hence, $\left[\boldsymbol{U}_{pp}^{(i,i)}\right]_{kj}$ can be computed efficiently using the FFT algorithm.

Although the ZF equalizer matrix is able to get rid of multiuser interference (MUI) from the same subcarrier in the current block i, we have to note that the complexity of the equalizer has almost doubled as, we now have an equivalent CIR having $(2L-1)$ taps. This is not an efficient equalizer as its complexity has now almost doubled. We will now try to get rid of IBI terms from the previous block as well as the interference terms from the past symbols in the current block by using a novel Decision Feedback based Interference cancellation(DFIC) mechanism in the next subsection.

4.1.4 Decision Feedback based Interference Cancellation (DFIC)

In the previous subsection, we used a ZF equalizer after TR processing to get rid of the Intra Block interference and Multi User Interference for the current block indexed i. However, this increased the complexity of the equalizer by almost 2 times. We now present a Decision Feedback based Interference Cancellation (DFIC) scheme which can be used to eliminate the interference terms arising from the past symbols based on the decision made on them. Before we present the algorithm, the notation that would be useful in understanding and implementing the algorithm is presented **Notation**

- Let $\mathbf{a} \cdot \mathbf{b}$ denote the scalar dot product between 2 vectors **a** and **b**.
- Let $\mathbf{a} = [a[0], a[1], ..., a[N-1]]^T$ and $\mathbf{b} = [b[0], b[1], ..., b[N-1]]^T$ be two vectors of length N. Then
  - $\Big[\mathbf{a}(n-L+1:n-1)\Big] = [a[n-L+1], a[n-L+2], ..., a[n-1]]^T$ is an $(L-1)$ length vector whose elements are the $(L-1)$ elements of the vector **a** preceding the element $a[n]$.
  - $\Big[\mathbf{a}(N-L+n+1:N-1) \quad \mathbf{b}(0:n-1)\Big] \triangleq \Big[a[N-L+n+1], a[N-L+n+2], ..., a[N-1], b[0], b[1], ..., b[n-3], b[n-1]\Big]^T$ is an $(L-1)$ length vector whose first $(L-n-1)$ elements are the last $(L-n-1)$ elements of vector **a** and last (n) elements are the first (n) elements of vector **b** respectively.

Let us now recall the definitions of few vectors that will be used in the algorithm.

1) Let $\mathbf{u}_{ij}^{DF} \triangleq [u_{ij}[2L-2], u_{ij}[2L-3], ..., u_{ij}[L]]^T$ for all $i \in [0, K-1]$ and $j \in [0, K-1]$. Recall the definition of $u_{ij}[2L-2]$ from eqn.(4.8).

2) Let $\mathbf{R}_k \triangleq \mathbf{y}_{k,i}^{TR}$ for all $k \in [0, K-1]$. Recall the definition of $\mathbf{y}_{k,i}^{TR}$ from equation (4.13).

3) Let n denote the index of the symbol for which the decision is being made. n increases from 0 to N-1 in the algorithm.

4) Let $x_{k,isi}$ denote the (L-1)-length vector containing L-1 symbols preceding the current symbol indexed by n for which the decision is being made. These L-1 symbols will contribute to the interference terms for the current symbol apart from the future L-1 symbols. As n varies, this window of L-1 preceding symbols in the vector $x_{k,isi}$ also moves forward, for all $k \in [0, K-1]$.

5) Let $y_{k,i}$ denote the N-length vector storing the current block of received symbols transmitted by the k^{th} transmit antenna after decision on the n^{th} symbol has been made. This vector $y_{k,i}$ is temporary and keeps changing as n varies. When $n = N-1$, we store this vector $y_{k,i}$ as $\bar{\mathbf{y}}_{k,i}^{TR,DF}$ which is the current block of received symbols from k^{th} transmit antenna after decision on all $N-1$ symbols have been made. $\bar{\mathbf{y}}_{k,i}^{TR,DF}$ will now be used as the previous block for DFIC carried out on $(i+1)^{th}$ block symbols.

Now we are ready to describe the algorithm.

Algorithm 1: Decision Feedback based Interference Cancellation

Result: Write here the result

$n = 0$

$\mathbf{R}_k = \mathbf{y}_{k,i}^{TR}$

$\mathbf{x}_{k,i-1} = IDFT(\bar{\mathbf{y}}_{k,i-1}^{TR,DF})$

while $n \leq (N-1)$ **do**

k =0

while $k \leq (K-1)$ **do**

$\mathbf{x}_{k,i,isi} = IDFT(y_{k,i})$

if $n \geq L-1$ **then**

$x_{k,isi} = [\boldsymbol{x}_{k,i,isi}(n-L+1:n-1)]$

else

$x_{k,isi} = [\boldsymbol{x}_{k,i-1}(N-L+n+1:N-1) \quad \boldsymbol{x}_{k,i,isi}(0:n-1)]$

end

k= k+1

end

k =0

while $k \leq (K-1)$ **do**

$R_{isi} = \sum_{j=0}^{K-1} (\mathbf{u}_{kj}^{DF} \cdot x_{j,isi})$

$\mathbf{R}_k[n] = \mathbf{R}_k[n] - R_{isi}$

$y_{k,i} = DFT(\mathbf{R}_k)$

if *n = (N-1)* **then**

$\bar{\mathbf{y}}_{k,i}^{TR,DF} = y_{k,i}$

end

k = k+1

end

n = n + 1

end

From the above algorithm, we are able to get rid of half the interference terms from the expression in eqn.(4.13). This is because, we are subtracting the interference caused due to previous $(L-1)$ bits when we are making a decision for the current bit. As a result, after DFIC, the eqn.(4.15) gets modified to

$$\bar{y}_{k,i}^{TR,DF}[p] = \underbrace{U_{kk,pp}^{(i,i)DF} d_{k,i}[p]}_{\text{Desired Signal}} + \underbrace{\sum_{q=0,q\neq p}^{N-1} U_{kk,pq}^{(i,i)DF} d_{k,i}[q]}_{\text{Intra Block Interference}} + \underbrace{\sum_{q=0}^{N-1} + U_{kk,pq}^{(i,i+1)DF} d_{k,i+1}[q]}_{\text{Inter Block Interference}}$$
$$+ \underbrace{\sum_{j=0,j\neq k}^{K-1} \sum_{q=0}^{N-1} \left(U_{kj,pq}^{(i,i)DF} d_{j,i}[q] + U_{kj,pq}^{(i,i+1)DF} d_{j,i+1}[q] \right)}_{\text{Multi User Interference}} + \underbrace{\bar{n}_{k,i}^{TR}[p]}_{\text{Noise}} + \underbrace{\bar{e}_{k,i}^{TR}[p]}_{\text{Detection error}} \tag{4.20}$$

In the above equation, we are able to get rid of interference terms from the previous block indexed by $(i-1)$. We are also able to get rid of intra block interference due to past symbols in the current block. Please note that the term $\bar{e}_{k,i}^{TR}[p]$ denotes the noise contribution due to making error in detecting the past symbols. Also note that the frequency domain equivalent channel matrices have now been modified to $U_{kj}^{(i,i)DF}$ and $U_{kj}^{(i,i+1)DF}$ as the equivalent channel matrices $\mathbf{U}_{kj}^{(i,i)}$ and $\mathbf{U}_{kj}^{(i,i+1)}$, themselves can treated as that of an L tap channel after accounting for interference from the last $L-1$ taps. The equivalent channel matrix $\mathbf{U}_{kj}^{(i,i-1)}$ can now be treated as a zero matrix for reasons stated above.

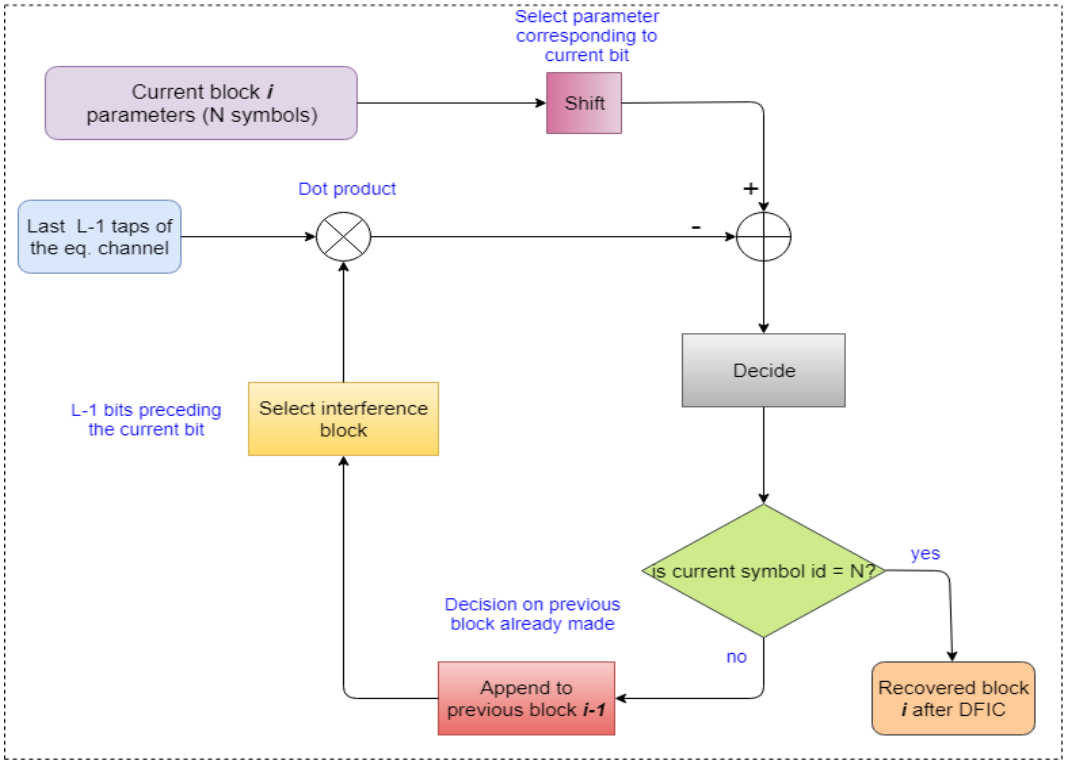

Figure 4.2: Simplistic flow diagram describing DFIC

The modified equivalent CIR matrices $U_{kj}^{(i,i)DF}$ and $U_{kj}^{(i,i+1)DF}$ can be constructed as described in eqn.(4.11) and eqn.(4.12) except that now the elements $u_{kj}[l] = 0$ for all $l \in [L, 2L-2]$. This is equivalent to saying that the equivalent channel impulse has been truncated from ($2L$-1) taps to L taps by making the last (L-1) taps equal to zero. This gives an improved BER performance compared to just TR processing described in Subsection 4.1.2. This will be validated in the next subsection where we present our simulation results. The performance can be improved further by implementing a ZF equalizer after DFIC.

4.1.5 Zero Forcing Equalization with L tap CIR

We have seen that DFIC improves the performance of the system by reducing the amount of interference experienced by the desired signal. This can be seen from the reduced number of interference terms in the eqn.(4.20) when compared to that in eqn.(4.15). The next question that arises is that can we do better than this? The answer is YES. We can implement a ZF equalizer after DFIC. We follow the same steps as described in Subsection 4.1.3 to generate the ZF matrix for a given subcarrier p. The only difference is that now the channel matrix $\mathbf{U}_{kj}^{(i,i)}$ has been replaced by $\mathbf{U}_{kj}^{(i,i),DF}$. Following the steps described in Subsection 4.1.3, we can write the expression for $\bar{\mathbf{y}}_i^{TR}[p] = [\bar{y}_{0,i}^{TR}[p], ..., \bar{y}_{K-1,i}^{TR}[p]]^T$ containing the p^{th} output of the DFT blocks for the different terminals as

$$\bar{\mathbf{y}}_i^{TR,DF}[p] = \boldsymbol{U}_{pp}^{(i,i),DF}\mathbf{d}_i[p] + \sum_{q=0,q\neq p}^{N-1} \boldsymbol{U}_{pq}^{(i,i),DF}\mathbf{d}_i[q] + \sum_{q=0}^{N-1} \boldsymbol{U}_{pq}^{(i,i+1),DF}\mathbf{d}_{i+1}[q] + \bar{\mathbf{n}}_i^{TR}[p] + \bar{e}_i^{TR}[p] \tag{4.21}$$

The term $\boldsymbol{U}_{pp}^{(i,i),DF}\mathbf{d}_i[p]$ contains the desired signals as well as the interference from i^{th} blocks of different mobile terminals transmitted in the same subcarrier frequency slot p. More specifically, the diagonal elements of $\boldsymbol{U}_{pp}^{(i,i),DF}$ correspond to the desired signal terms and the off-diagonal elements correspond to the interference terms. The ZF equalizer matrix is the inverse of the matrix $\boldsymbol{U}_{pp}^{(i,i),DF}$. The recovered data for the p^{th} subcarrier after ZF equalization can be written as

$$\hat{\mathbf{d}}_i^{DF}[p] = \left(\boldsymbol{U}_{pp}^{(i,i),DF}\right)^{-1} \bar{\mathbf{y}}_i^{TR,DF}[p]. \tag{4.22}$$

We now describe an easy way to generate the matrix $\boldsymbol{U}_{pp}^{(i,i),DF}$. Recall that

$$\left[\boldsymbol{U}_{pp}^{(i,i),DF}\right]_{kj} = U_{kj,pp}^{(i,i),DF} = \left[\bar{\mathbf{U}}_{k,j}^{(i,i),DF}\right]_{pp} = \mathbf{f}_p^T \mathbf{U}_{kj}^{(i,i),DF} \mathbf{f}_p^*, \tag{4.23}$$

where $\mathbf{f}_p$ is the $(p-1)^{th}$ row of the DFT matrix. After some algebraic manipulations $\left[\boldsymbol{U}_{pp}^{(i,i),DF}\right]_{kj}$ can be found as

$$\left[\boldsymbol{U}_{pp}^{(i,i),DF}\right]_{kj} = U_{kj,pp}^{(i,i),DF} = \mathbf{f}_p^T \mathbf{U}_{kj}^{(i,i),DF} \mathbf{f}_p^* = \frac{1}{N} \sum_{l=0}^{L-1} \Big(N - |l-(L-1)|\Big) u_{kj}[l] e^{-j\frac{2\pi\left(l-(L-1)\right)p}{N}}. \tag{4.24}$$

Based on the above expression, $\left[\boldsymbol{U}_{pp}^{(i,i)}\right]_{kj}$ is equal to the p^{th} coefficient of the N-point DFT of the signal $u'_{kj} \triangleq \frac{\left(N-|l-(L-1)|\right)}{N} u_{kj}[l] e^{j\frac{2\pi(L-1)p}{N}}$ for all $l \in [0, L-1]$. Hence, $\left[\boldsymbol{U}_{pp}^{(i,i),DF}\right]_{kj}$ can be computed efficiently using the FFT algorithm.

Therefore, we have been able to reduce the ZF equalizer complexity by half compared to the ZF equalizer implemented in Subsection 4.1.3. We present the simulation results for our system in the next section

4.2 Simulation Results

In this section we discuss the simulation results obtained for the 4 cases presented in the previous section namely:

- Case 1: OFDM without CP followed by TR (denoted by "TR" in the plots).
- Case 2: OFDM without CP followed by TR and ZF equalizer with $(2L-1)$ taps(denoted by "TR ZF 2L-1" in the plots)
- Case 3: OFDM without CP followed by TR and DFIC (denoted by "TR DFE" in the plots).
- Case 4: OFDM without CP followed by TR, DFIC and ZFequalizer with L taps (denoted by "TR DFE ZF L" in the plots).

For all our simulations, we consider an DFT size of $N = 256$, ie, there are 256 subcarriers. We assume that all 256 subcarriers are utilized. We consider BPSK data symbols $\mathbf{d}_{k,i}$ for our simulations, however the results are valid for any QAM modulation

scheme. All the simulations are run for a total of 10^6 symbols and the Channel is assumed to be stationary for every 1000 symbols.

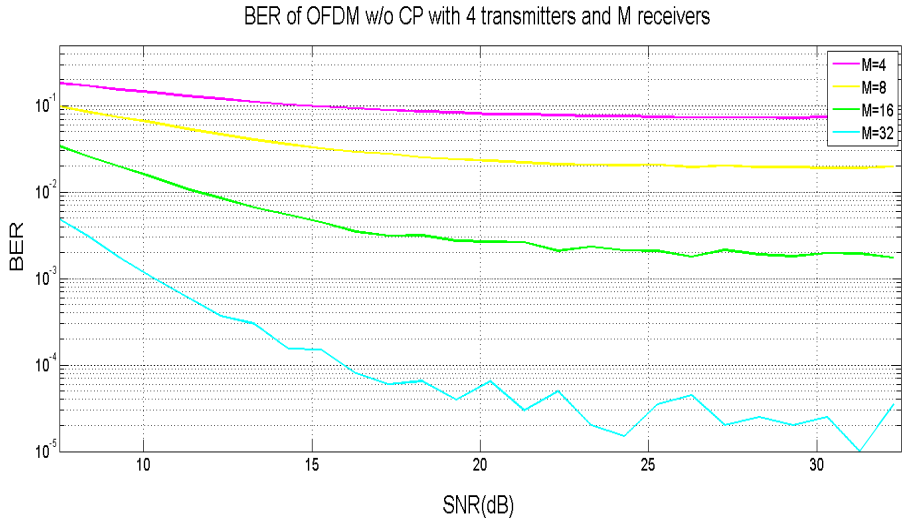

Figure 4.3: Receive diversity for 50 tap channel

In Figure 4.3, we can see BER of OFDM without CP followed by TR system for the case where there are 4 transmit mobile stations and 50 tap channel. From the plot we can see that there is obvious receive diversity benefit as we increase the number of receiver antennas at the base station. Another insight from the plot is that BER curve saturates after a certain SNR level depending on the number of receiver antennas. This validates the theoretical knowledge that SINR saturates for OFDM w/o CP TR system when the number of receive antennas are finite as presented in Aminjavaheri *et al.* (2017).

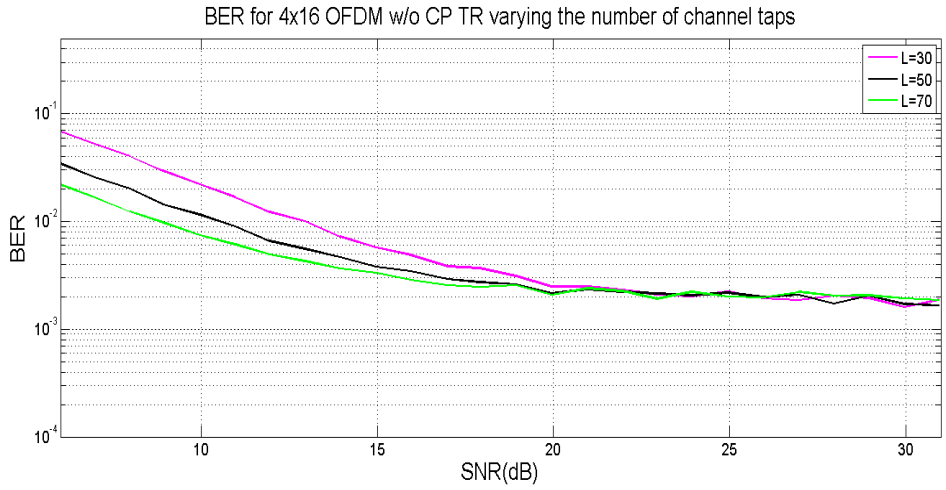

Figure 4.4: BER vs SNR for 16x4 with varying channel taps L

In Figure 4.4, we compare the BER performance of OFDM without CP followed by TR system for a given configuration of 16x4 MIMO system by varying the number

of channel taps. It is observed that for small SNR value, the BER is better when the number of channel taps L is large. However, for a given configuration KxM, the BER saturates to the same value for all values of L.

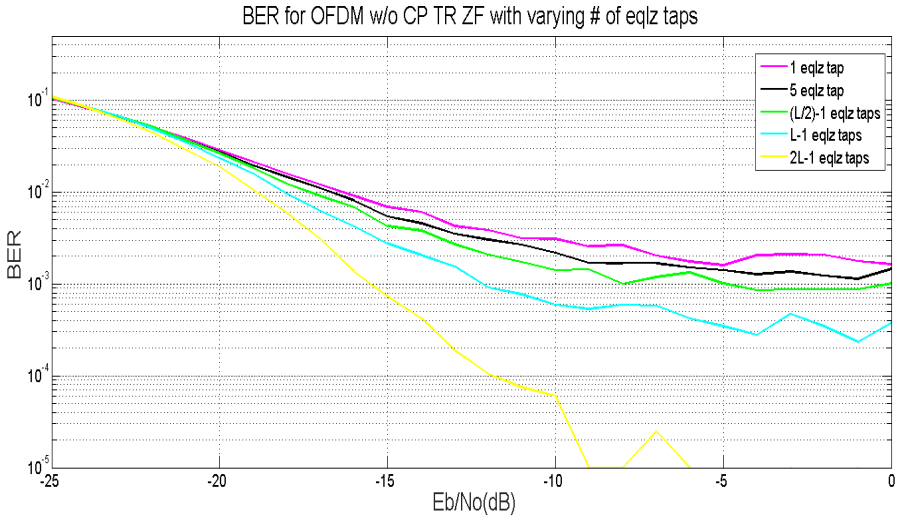

Figure 4.5: BER for 16x4 OFDM w/o CP TR ZF with varying number of equalizer taps for L=20 channel taps

We next consider Case 2, where we implement a ZF equalizer after TR processing at the receiver with the hope of improving the performance. The ZF equalizer matrix is constructed using all $(2L-1)$ taps of the equivalent CIR after TR processing. Although this improves the performance of the system in terms of BER, but it also increases the equalizer complexity by almost 2 times. One advantage of TR is the temporal focussing effect, by which most of the energy is concentrated around the central tap of the equivalent CIR. As a result, we can construct an equalizer considering only the central taps of the equivalent CIR. In other words, we consider a truncated CIR for constructing the ZF equalizer matrix. Figure 4.5 shows the BER performance for 16x4 OFDM w/o CP TR ZF system where we vary the number of central taps used for constructing the ZF equalizer matrix. In the legend, L stands for the number of channel taps which is equal to 20 for this simulation. As expected, there is a trade off between complexity of the ZF equalizer and the BER performance. The BER performance improves as we consider more and more number of central taps for constructing the ZF equalizer matrix. The best performance is obtained when all $(2L-1)$ taps of the equivalent CIR is used for constructing the ZF equalizer matrix.

Next, we consider Case 3 and Case 4, where instead of using a ZF equalizer based on (2L-1) taps, we implement a DFIC block after TR as described in Subsection 4.1.4.

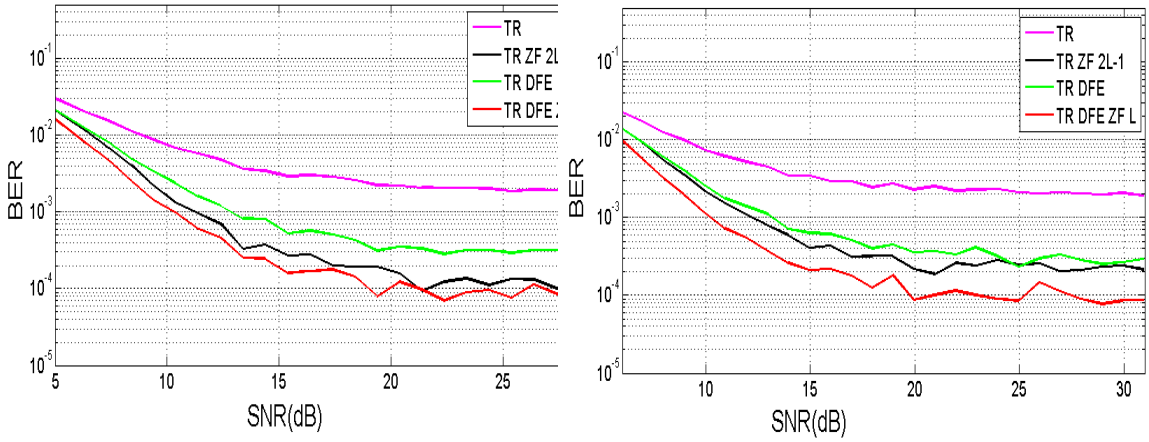

(a) 50 tap channel

(b) 70 tap channel

Figure 4.6: BER vs SNR for 16x4 MIMO system

This helps to get rid of interference terms from the past $(L-1)$ bits, decision on which has already been made. From Figures 4.6(a) and 4.6(b), we can see that green curve "TR DFE" which stands for the BER for the recovered bits after DFIC block performs much better than the OFDM w/o CP TR curve "TR" depicted by pink. After the DFIC processing,we can improve the BER further by implementing a ZF Equalizer based only on the first L taps of the equivalent CIR as described in Subsection 4.1.5. This is because interference originating due to the last $(L-1)$ taps have already been cancelled by the DFIC block. Comparing the position of the red curves in Figures 4.6(a) and 4.6(b) we can see that the ZF equalizer based on L taps improves the BER performance as the number of channel taps increases. Also, it is able to achieve a better BER performance for system compared to that of OFDM w/o CP TR followed by ZF equalizer based on $(2L-1)$ taps(shown by black curve "TR ZF 2L-1") described in Subsection 4.1.3. This is true for the case where the number of channel taps L is greater than 40 for our configuration of 16x4 MIMO system considered for the simulation.

To summarize, by using a DFIC block followed by a ZF Equalizer based on L taps, we are able to achieve a better BER performance compared to the BER performance of conventional ZF Equalizer based on $(2L-1)$ taps. However, this is valid only if the number of channel taps are large enough(≥ 40 for our simulation). Hence this is a possible solution for multipath channels with large delay spread compared to the time resolvability window or the sampling period.

In Figures 4.7(a) and 4.7(b), the BER performance of Conventional OFDM with CP and OFDM without CP have also been plotted to describe a complete picture of what

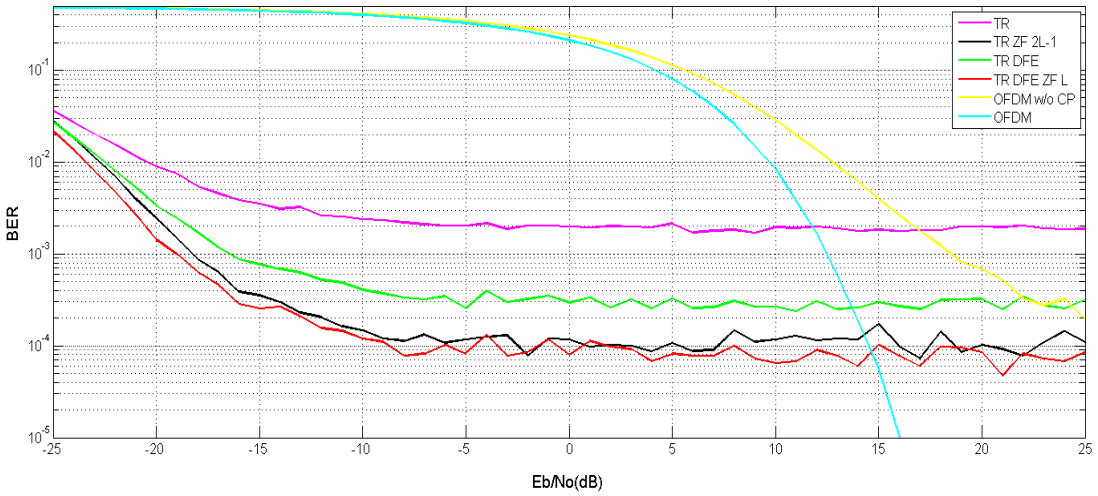

(a) 50 tap channel

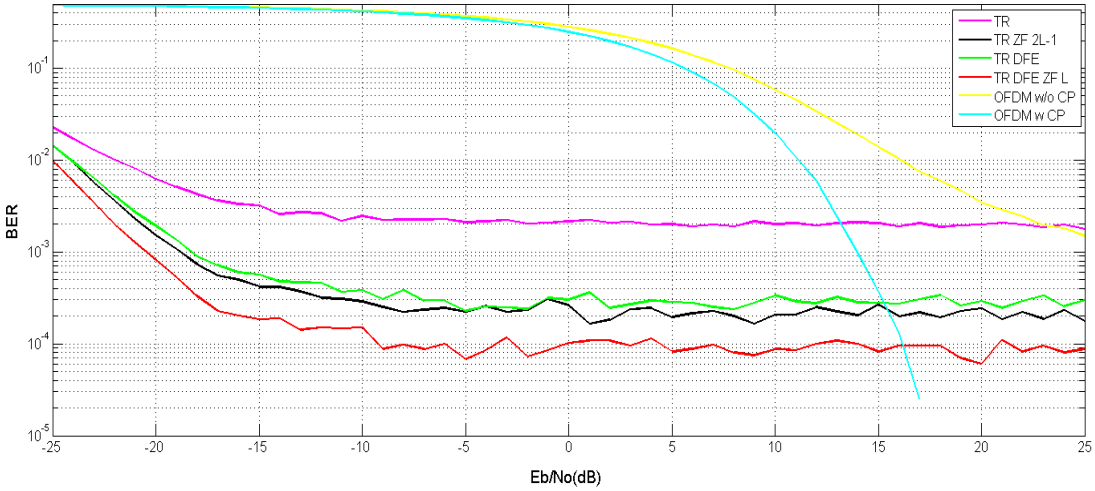

(b) 70 tap channel

Figure 4.7: Comparison of different OFDM schemes

we have achieved. They are denoted by "OFDM" and "OFDM w/o CP" respectively in the legend. This has been done to allow a comprehensive comparison of all the systems implemented in this Chapter. We can clearly see that our proposed system of OFDM w/o CP followed by TR, DFIC and ZF Equalizer achieves the best BER in bad channel conditions(small value of E_b/N_0) when the number of channel taps are large. As a result, this system can be used as an alternate for conventional OFDM with CP during poor channel conditions. Let V dB denote the cross over point E_b/N_0 value when the Conventional OFDM with CP's BER curve crosses the red curve in Figures 4.7(a) and 4.7(b). We can define poor channel conditions as the region in the BER curve when E_b/N_0 is between -5 dB and VdB. This crossover point moves towards the right as the number of channel taps L increases, thus making our system more and more attractive

for operation in this regime.

We are able to nullify the effect of interference from the previous $(L-1)$ bits with the help of DFIC. Can we improve the performance further? In order to inquire this, we tried hybrid methods by allowing 20% Zero Padding after every block. This helps to reduce the interference due to the future block symbols. The simulation results is shown in Figure 4.8 below for a 50 tap channel. We see that the BER improves marginally compared to the BER without zero padding. The dotted lines denote the case where no zero padding is done and the solid lines denote the case where 20% zero padding is employed.

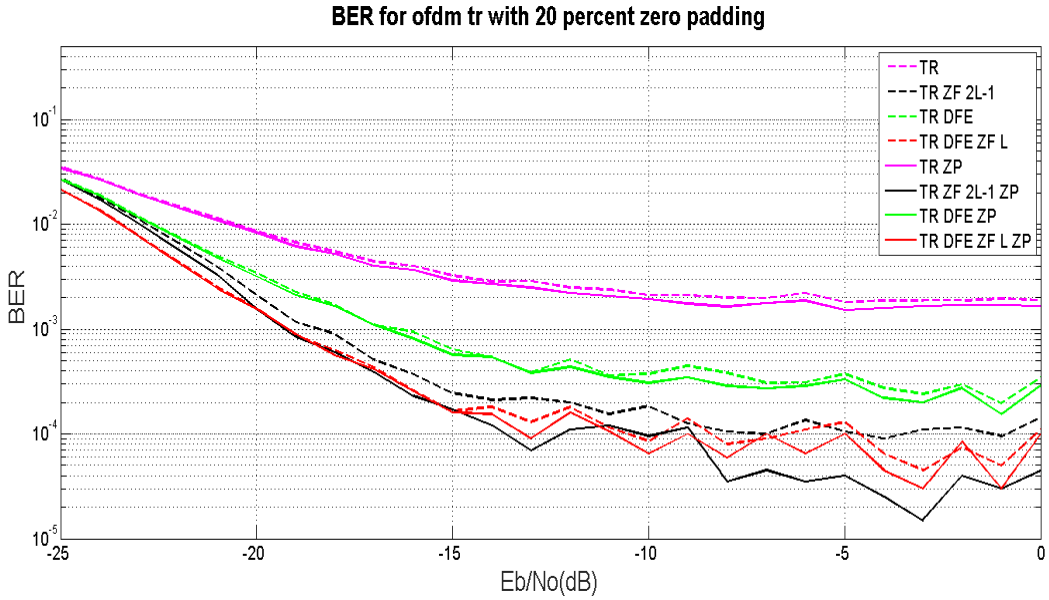

Figure 4.8: OFDM schemes w and w/o ZP for 16x4 MIMO with 50 tap channel

One possible query in the mind of the readers can be, why are we considering negative E_b/N_0 in our simulations as described in the BER plots of Figure 4.7 (a) and (b). The reason for this is that although E_b/N_0 is negative, the corresponding SNR and SINR are positive due to the huge receive diversity gain achieved by TR processing. This can be seen from the SINR and SNR plots in Figures 4.9(a) and 4.9(b) respectively. We can observe that SINR saturates as E_b/N_0 becomes positive whose direct consequence is the BER saturation, but SNR increase linearly with E_b/N_0.

However, a major challenge is the Channel estimation in poor channel conditions during the channel probing phase of TR. This can be overcome by using a pilot signal whose length is greater than L. This can help us to estimate channel by sending pseudo random pilot sequence whose correlation peak can be used to estimate the channel.

(a) SINR vs E_b/N_0 (b) SNR vs E_b/N_0

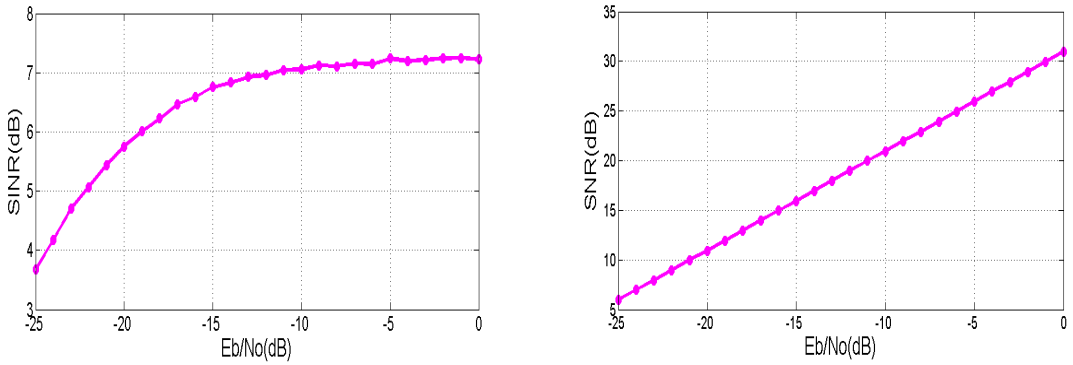

Figure 4.9: SINR and SNR for 16x4 OFDM w/o CP in 70 tap channel

However, this incurs some overhead. But as mentioned in the Introduction Chapter, we consider perfect knowledge of channel for our study of TR throughout this thesis. Perhaps, efficient channel estimation in poor channel conditions can be treated as potential direction of future research.

CHAPTER 5

Conclusions and Future Work

Two implementations of Time Reversal (TR) processing have been studied: at the transmitter and at the receiver. From the study of TR processing at the transmitter, we see that TR MIMO performs better than TR SIMO in terms of BER, due to the superior transmit diversity gain which is able to overpower the degradation due to increased Multi User Interference (MUI). For a particular configuration of KxM TR MIMO system, on increasing the number of channel taps results in an improvement in BER performance. The BER can be further improved by using a ZF equalizer after TR processing, but this does not yield significant improvement. One of the major challenges of TR processing at the transmitter studied in this thesis is that it incurs considerable overhead due to the upsampling done before pulse shaping. We try to overcome this challenge by using OFDM technique where adjacent symbols are sent over different subcarrier frequencies which are orthogonal to each other.

We also study (uplink) TR processing at the receiver (Base station) as it provides us with the opportunity to leverage the availability of computational resources at the Base station. This can be used to carry out the complex ZF Equalization and Decision Feedback based Interference Cancellation after TR processing. We begin by implementing OFDM w/o CP followed by TR and ZF equalizer using all $(2L-1)$ taps of the equivalent CIR. Through the use of a DFIC block followed by ZF equalizer based on L taps, we are able to lower the BER saturation floor further if the number of channel taps L is large enough. We also compare the performance of this new system with that of conventional OFDM with CP. It is observed that the proposed system performs better than conventional OFDM with CP in poor channel conditions. But this brings about the need for efficient Channel estimation in poor channel conditions (low SNR).

Potential sources for future research work can be coming up with an efficient way of reliable channel estimation in poor channel conditions. One interesting idea to work on is the use of TR processing for channel shortening applications. This will help in reducing the effect of ISI suffered in large tap channels. Another interesting idea to

explore is that of TR processing in underwater acoustics application. There has been some study about TR in underwater acoustic channels with OFDM modulation by Edelmann *et al.* (2005) and Gomes and Barroso (2004). Underwater acoustic channels have small bandwidth, and hence, a small number of taps. Another interesting application of TR technique is indoor localization or position detection Chen *et al.* (2016) where TR signatures of CIR from different locations in an indoor setting are correlated with the incoming signal to estimate the location from which the signal originated. Ray Liu and his team has been carrying out active research in this area. Some of the interesting solutions developed using time reversal by his team most recently include TR-Breath Chen *et al.* (2018) where TR technique is used to monitor the breathing rate of a person, and TRIEDS Xu *et al.* (2017*b*) which deals with wireless event detection. The most recent addition to their work is TR based human identification Xu *et al.* (2017*a*), which eliminates need for physical contact between human and identification device to capture human biometric traits.

Overall, TR is a useful DSP tool that can provide substantial advantages in a diverse set of communication applications. The goal of this thesis has been to document the benefits of TR processing in MIMO and OFDM contexts.

REFERENCES

1. **Aminjavaheri, A.**, **A. Farhang**, **A. Rezazadehreyhani**, **L. E. Doyle**, and **B. Farhang-Boroujeny** (2017). Ofdm without cp in massive mimo. *IEEE Transactions on Wireless Communications*, **16**(11), 7619–7633. ISSN 1536-1276.

2. **Bogert, B.** (1957). Demonstration of delay distortion correction by time-reversal techniques. *IRE Transactions on Communications Systems*, **5**(3), 2–7. ISSN 0096-2244.

3. **Bottomley, G. E.** and **S. Chennakeshu** (1998). Unification of mlse receivers and extension to time-varying channels. *IEEE Transactions on Communications*, **46**(4), 464–472. ISSN 0090-6778.

4. **Chen, C.**, **Y. Chen**, **Y. Han**, **H. Q. Lai**, **F. Zhang**, and **K. J. R. Liu** (2017). Achieving centimeter-accuracy indoor localization on wifi platforms: A multi-antenna approach. *IEEE Internet of Things Journal*, **4**(1), 122–134. ISSN 2327-4662.

5. **Chen, C.**, **Y. Han**, **Y. Chen**, **H. Q. Lai**, **F. Zhang**, **B. Wang**, and **K. J. R. Liu** (2018). Tr-breath: Time-reversal breathing rate estimation and detection. *IEEE Transactions on Biomedical Engineering*, **65**(3), 489–501. ISSN 0018-9294.

6. **Chen, C.**, **Y. Han**, **Y. Chen**, **F. Zhang**, and **K. J. R. Liu**, Time-reversal indoor positioning with centimeter accuracy using multi-antenna wifi. *In 2016 IEEE Global Conference on Signal and Information Processing (GlobalSIP)*. 2016.

7. **Chen, Y.**, **F. Han**, **Y. H. Yang**, **H. Ma**, **Y. Han**, **C. Jiang**, **H. Q. Lai**, **D. Claffey**, **Z. Safar**, and **K. J. R. Liu** (2014). Time-reversal wireless paradigm for green internet of things: An overview. *IEEE Internet of Things Journal*, **1**(1), 81–98. ISSN 2327-4662.

8. **Edelmann, G. F.**, **H. C. Song**, **S. Kim**, **W. S. Hodgkiss**, **W. A. Kuperman**, and **T. Akal** (2005). Underwater acoustic communications using time reversal. *IEEE Journal of Oceanic Engineering*, **30**(4), 852–864. ISSN 0364-9059.

9. **Farhang, A.**, **A. Aminjavaheri**, **A. R. Reyhani**, **L. E. Doyle**, and **B. Farhang-Boroujeny**, Time reversal with post-equalization for ofdm without cp in massive mimo. *In 2016 International Symposium on Wireless Communication Systems (ISWCS)*. 2016.

10. **Gomes, J.** and **V. Barroso**, Time-reversed ofdm communication in underwater channels. *In IEEE 5th Workshop on Signal Processing Advances in Wireless Communications, 2004.*. 2004.

11. **Han, Y.**, **Y. Chen**, **B. Wang**, and **K. J. R. Liu** (2016). Time-reversal massive multipath effect: A single-antenna x201c;massive mimo x201d; solution. *IEEE Transactions on Communications*, **64**(8), 3382–3394. ISSN 0090-6778.

12. **Hieu Nguyen, T. K. N. K. M. F. Z., Van Duc Nguyen** and **T. Kaiser**, On the performance of the time reversal sm-mimo-uwb system on correlated channels. *In International Journal of Antennas and Propagation*, volume 2012. 2012. ISSN 929018.

13. **Lindskog, E.** and **D. Flore**, Time-reversal space-time block coding and transmit delay diversity-separate and combined. *In Conference Record of the Thirty-Fourth Asilomar Conference on Signals, Systems and Computers (Cat. No.00CH37154)*, volume 1. 2000. ISSN 1058-6393.

14. **Lindskog, E. D.** and **A. J. Paulraj**, Time-reversal block transmit diversity system for channels with intersymbol interference and method. US 7362815 B2. 2000. URL `https://lens.org/089-912-755-113-793`.

15. **Nguyen, H.**, **Z. Zhao**, **F. Zheng**, and **T. Kaiser** (2010). Preequalizer design for spatial multiplexing simo-uwb tr systems. *IEEE Transactions on Vehicular Technology*, **59**(8), 3798–3805. ISSN 0018-9545.

16. **Nguyen, H.**, **F. Zheng**, and **T. Kaiser**, Antenna selection for time reversal mimo uwb systems. *In VTC Spring 2009 - IEEE 69th Vehicular Technology Conference*. 2009. ISSN 1550-2252.

17. **Viterbi, A. J.** (1998). An intuitive justification and a simplified implementation of the map decoder for convolutional codes. *IEEE Journal on Selected Areas in Communications*, **16**(2), 260–264. ISSN 0733-8716.

18. **Wang, L.**, **R. Li**, **C. Cao**, and **G. L. StÃijber** (2016). Snr analysis of time reversal signaling on target and unintended receivers in distributed transmission. *IEEE Transactions on Communications*, **64**(5), 2176–2191. ISSN 0090-6778.

19. **Xu, Q.**, **Y. Chen**, **B. Wang**, and **K. J. R. Liu** (2017*a*). Radio biometrics: Human recognition through a wall. *IEEE Transactions on Information Forensics and Security*, **12**(5), 1141–1155. ISSN 1556-6013.

20. **Xu, Q.**, **Y. Chen**, **B. Wang**, and **K. J. R. Liu**, Time reversal based wireless events detection. *In 2017 IEEE International Conference on Acoustics, Speech and Signal Processing (ICASSP)*. 2017*b*.